

This discussion paper is/has been under review for the journal Biogeosciences (BG).
Please refer to the corresponding final paper in BG if available.

Swept under the carpet: the effect of organic matter burial in global biogeochemical ocean models

I. Kriest and A. Oschlies

Helmholtz-Zentrum für Ozeanforschung Kiel (GEOMAR), Düsternbrooker Weg 20, 24105 Kiel, Germany

Received: 21 June 2013 – Accepted: 24 June 2013 – Published: 3 July 2013

Correspondence to: I. Kriest (ikriest@geomar.de)

Published by Copernicus Publications on behalf of the European Geosciences Union.

BGD

10, 10859–10911, 2013

Organic matter burial in global biogeochemical ocean models

I. Kriest and A. Oschlies

[Title Page](#)

[Abstract](#)

[Introduction](#)

[Conclusions](#)

[References](#)

[Tables](#)

[Figures](#)

[⏪](#)

[⏩](#)

[◀](#)

[▶](#)

[Back](#)

[Close](#)

[Full Screen / Esc](#)

[Printer-friendly Version](#)

[Interactive Discussion](#)



5 (“OMZs”), which, although covering only a small volume of the global ocean, are crucial for controlling the marine nitrogen inventory. OMZs are notoriously difficult to reproduce in numerical models, and their representation seems particularly sensitive to changes in the parameterizations of remineralization processes (Oschlies et al., 2008; Bianchi et al., 2013). In global models such as those used to predict the evolution of OMZ under global warming (e.g. Duteil and Oschlies, 2011; Stramma et al., 2012), remineralization at low oxygen levels has been parameterized in many different ways.

10 Reduction or cessation of remineralization in the absence of oxygen seems to be a plausible choice for models that focus on the open ocean. However, in such models sinking detritus may accumulate below suboxic zones and, according to our own sensitivity experiments, reach unrealistically high concentrations. This suggests that there is (i) too intense export production or (ii) too little lateral mixing of the remineralization signal with surrounding water masses, a problem sometimes referred to as nutrient trapping. A third explanation for too intense accumulation of remineralization products in water columns associated with eastern tropical upwelling regions could be the neglect of burial of particulate organic matter in the sediment.

15 Despite the fact, that global burial of organic matter in the sediments is rather small compared to biogeochemical fluxes in the water column, and has therefore often been neglected – more specifically: treated as absent – in global biogeochemical ocean models (e.g. Matear and Hirst, 2003), it nevertheless influences biogeochemical processes locally and, on long time scales, will impact tracer distributions in the entire water column and, on even longer time scales, may affect the oxygen content of the atmosphere (Najjar et al., 2007).

25 Inspection of various published biogeochemical models reveals that burial and also remineralization in low-oxygen waters are treated often in very different ways in different models. For example, in the “PISCES” model (as described in the appendix of Aumont and Bopp, 2006), which includes both aerobic as well as anaerobic remineralization (the former depending on oxygen, the latter on both oxygen and nitrate), remineralization of organic matter ceases in the absence of oxygen. In this model sinking organic

Organic matter burial in global biogeochemical ocean models

I. Kriest and A. Oschlies

[Title Page](#)[Abstract](#)[Introduction](#)[Conclusions](#)[References](#)[Tables](#)[Figures](#)[Back](#)[Close](#)[Full Screen / Esc](#)[Printer-friendly Version](#)[Interactive Discussion](#)

result in a “Martin” flux profile (Martin et al., 1987, i.e. $F \propto z^{-b}$) with an exponent b of 0.858 (experiment “ref” of Kriest et al., 2012).

Detritus that enters the last box remains as detritus and remineralizes with its given remineralization rate of 0.05 d^{-1} . Similar to Marchal et al. (1998); Matear and Hirst (2003) and Najjar et al. (2007), KKO12 assumed that for oxygen concentrations below $4 \text{ mmol O}_2 \text{ m}^{-3}$ remineralization of organic matter continues, but does not use any oxygen, thereby mimicking the consumption of other, non-specified oxidants such as nitrate.

A new model feature investigated here is burial of detritus at the sea floor. In order to satisfy global mass conservation of phosphorus, buried detrital phosphorus is resupplied as phosphate via river runoff, while the non-buried detritus is resuspended in the water column. In the following we describe this model modification in more detail.

2.1 Parameterization of benthic burial

Let $0 \leq f_B \leq 1$ be the fraction of organic matter reaching the sea floor which is buried permanently in the sediment. For $f_B = 0$ (no burial), detritus remains in the last box, where it slowly remineralizes, further depleting the oxygen (e.g. in Schmittner et al., 2008; Kriest et al., 2010). In the opposite case, $f_B = 1$ (e.g. in the PISCES model; Aumont and Bopp, 2006) implies complete burial of organic matter reaching the the sea floor. Between these two extremes f_B may vary, among other things, with flux to the sea floor, water depth, or bottom water conditions. For example, Burdige (2007) suggested to relate the so-called burial efficiency, f_B , to the amount of organic matter falling onto the sea floor (F_R ; here in $\text{mmol P m}^{-2} \text{ d}^{-1}$) via

$$f_B = \alpha F_R^{\beta-1} \quad (1)$$

according to which the amount of burial in the sediment, F_B , can be described via

$$F_B = f_B F_R = \alpha F_R^\beta \quad (2)$$

BGD

10, 10859–10911, 2013

Organic matter burial in global biogeochemical ocean models

I. Kriest and A. Oschlies

Title Page

Abstract

Introduction

Conclusions

References

Tables

Figures

⏪

⏩

◀

▶

Back

Close

Full Screen / Esc

Printer-friendly Version

Interactive Discussion



2.3 Phosphorus budget closure via river runoff

The above parameterization of permanent burial of organic matter in marine sediments removes P from the oceanic pelagic system. To account for mass preservation on long time scales, we re-supply it again via river runoff, using a subset of river runoff data of Table 2 of Perry et al. (1996), i.e. the volumetric flow rates of the largest rivers in the world. We did not use direct P- or N-discharge rates, because these may exhibit a strong anthropogenic influence e.g. due to fertilizers, and therefore may not correspond to the steady-state system envisaged here.

Instead, we calculated the volumetric runoff of each river as a fraction of global runoff, and distribute it vertically over the entire water column of the model boxes that receive river runoff, i.e. in the vicinity of a river mouth (thereby mimicking unspecified processes, such as frontal dynamics). To combine P loss due to burial and P gain due to river runoff, during runtime the loss of P due to burial in the sediment is integrated over total model area and – for computational efficiency – over one year. The resulting global annual loss is then resupplied continuously over the following year. More details about data treatment can be found in Appendix B.

2.4 The circulation field

Kriest et al. (2012) used circulation fields derived from a relatively coarsely resolved ($2.8^\circ \times 2.8^\circ$, 15 vertical levels) circulation model (here referred to as “MIT2.8”) to examine the effect of different biogeochemical parameterizations on the spatial distribution of phosphate and oxygen. Because ventilation pathways and coastal processes may be important for the formation and persistence of OMZs, we here focus on biogeochemical models simulated with transport derived from the “Estimating the Circulation and Climate of the Ocean” (ECCO) project, which provides circulation fields that yield a best fit to hydrographic and remote sensing observations over the 10 yr period 1992 through 2001 on a rather fine spatial resolution of $1^\circ \times 1^\circ$ horizontal resolution with 23 vertical levels (Stammer et al., 2004).

10866

BGD

10, 10859–10911, 2013

Organic matter burial in global biogeochemical ocean models

I. Kriest and A. Oschlies

Title Page

Abstract

Introduction

Conclusions

References

Tables

Figures

⏪

⏩

◀

▶

Back

Close

Full Screen / Esc

Printer-friendly Version

Interactive Discussion



2.5 Model experiments

We first examine the effect of the finer resolution and different circulation inherent in the ECCO matrix via comparison to the results obtained with the “coarser” MIT2.8 matrix. For both configurations, ECCO and MIT2.8, we have carried out a set of seven experiments, where we varied the flux exponent from 0.429 up to 1.287 in model “NPZD-DOP” of KKO12 (hereafter named “CTL”; see also Table 1). In these initial model simulations, burial is not included and resuspension of any detritus hitting the bottom is assumed, i.e. we apply option (ii) of Sect. 2.2.

We then evaluate different biogeochemical models in the ECCO configuration. Starting from the model CTL, in setup “BUR” we introduce burial via Eq. (2), with our best fit to our sediment data compilation, $\alpha = 1.6828 \text{ [mmol P m}^{-2} \text{ d}^{-1}]^{1-\beta}$ and $\beta = 1.799$. We further test the effect of a weak relationship between rain rate and burial using the open-ocean composite described above ($\alpha = 0.0176 \text{ [mmol P m}^{-2} \text{ d}^{-1}]^{1-\beta}$, $\beta = 1.022$). This setup is named “WBUR”. We finally carried out experiments with the algorithm suggested by Dunne et al. (2007), here denoted by “DUNNE”. To examine the effect of instantaneous benthic remineralization, as described above we also present experiments where all organic matter hitting the sea floor is immediately remineralized (“INST”).

As in KKO12, for each of the setups we have carried out a set of four experiments where we varied the flux exponent b from the reference (“ref”) experiment ($b = 0.858$) upwards to 1.0725 (experiment “s2” of KKO12; hereafter named experiment “slow”) and 1.287 (“s1” of KKO12; hereafter named “very slow”) and downwards to 0.644 (“s3” of KKO12; hereafter named “fast”) and 0.429 (“s4” of KKO12; hereafter named “very fast”; see also Table 1).

2.6 Model assessment

Results from model experiments are compared to the gridded ($1^\circ \times 1^\circ$) analyzed set of observations of phosphate and oxygen compiled by Garcia et al. (2006a) and Garcia

BGD

10, 10859–10911, 2013

Organic matter burial in global biogeochemical ocean models

I. Kriest and A. Oschlies

Title Page

Abstract

Introduction

Conclusions

References

Tables

Figures

⏪

⏩

◀

▶

Back

Close

Full Screen / Esc

Printer-friendly Version

Interactive Discussion



et al. (2006b). We mapped the data set to the respective model resolution. By doing so, we release the coarser model from the penalties imposed by its lack of resolution, and investigate just the errors due to its numerical diffusion (e.g. due to upstream schemes in particle flux; see Kriest and Oschlies, 2011), circulation and biogeochemistry. To assess the models' performance with respect to dissolved tracers, we apply a global misfit function based on the volume-weighted root-mean-square-error, as described in KKO12. Data sets used for comparison to simulated pelagic and benthic fluxes will be described in the respective section.

3 Impact of spatial resolution and physics

The volumetric distribution of global phosphate is quite similar in both control model configurations (Fig. 2, upper panels). The overall mismatch of ECCO with respect to phosphate is lower than that for MIT2.8, but the sensitivity to changes in the remineralization length scale is very similar among the two different models driven by different circulation fields (Fig. 2b). The same increase in settling speed (e.g., "ref" to "fast") has a larger effect in MIT2.8 than in ECCO. In the former, this increase results in a much more homogenous distribution of phosphate, with an overestimate of water volume with rather low and rather high concentrations. This effect is not so pronounced in ECCO.

Greater differences appear when comparing the oxygen distributions (Fig. 2, lower panels). First, the remineralization length scale shows a strong impact on the simulated oxygen distribution, with a strong volumetric overestimate of low oxygen regions when sinking is fast. Second, in MIT2.8 we find a bimodal volumetric distribution of oxygen, whereas the oxygen distribution in ECCO is more or less unimodal and, in this respect, in better agreement with WOA05. Particularly the fast-sinking scenarios of MIT2.8 show oxygen concentrations below $50 \text{ mmol O}_2 \text{ m}^{-3}$ in large parts of the deep ocean, causing a peak of ocean volume with rather low concentrations. Reasons for differences among the two model configurations may be differences in the circulation fields, but also the

Title Page

Abstract

Introduction

Conclusions

References

Tables

Figures



Back

Close

Full Screen / Esc

Printer-friendly Version

Interactive Discussion

differences in the vertical resolution, causing a higher numerical diffusion in MIT2.8 (see also Kriest and Oschlies, 2011).

For the biogeochemical model variations considered, ECCO fits observed oxygen much better than MIT2.8, while its results show the same sensitivity to changes in the remineralization length scale. In the following sections we will focus on results from simulations of the ECCO configuration.

4 Impact of burial and benthic remineralization on pelagic tracers

Similar to results obtained by Kwon and Primeau (2006) and Kriest et al. (2012), simulated nutrient concentrations in older waters such as in the mesopelagic and bathypelagic North Pacific are very sensitive to changes in the remineralization length scale in our models “CTL” and “INST”. Further, Kwon and Primeau (2006) found that nutrients in the Eastern Equatorial Pacific (hereafter name EEP) are particularly sensitive to changes in organic matter production and decay terms. As we will show below, in our model experiments these two regions also appear particularly sensitive to assumptions about burial and remineralization. Besides investigating the nutrient and oxygen concentration above the sea floor, we will therefore, in the following, mostly focus on phosphate and oxygen in these two regions.

Obviously, we can expect effects of benthic burial and remineralization on the nutrient and oxygen concentration near the sea floor, as depicted in Fig. 3 for models INST, CTL and BUR simulated with moderate (scenario “ref”) particle sinking speed. Both model INST and CTL are very similar, as they predict far too high bottom-water phosphate concentrations in the Pacific Ocean, and, correspondingly, far too low bottom-water oxygen concentrations. This mismatch gets worse for faster settling speed (no figure). Introducing burial improves the match to observed pelagic tracer fields, both with respect to phosphate and oxygen. The differences among the different scenarios decrease for slower settling speeds, where the models show a similar fit for phosphate,

Title Page

Abstract

Introduction

Conclusions

References

Tables

Figures

⏪

⏩

◀

▶

Back

Close

Full Screen / Esc

Printer-friendly Version

Interactive Discussion



and model BUR yields even slightly too high oxygen in the deep Pacific Ocean (no figure).

The introduction of burial also affects the simulated distribution of phosphate and oxygen in upper parts of the water column, as evident from a section along the “conveyor belt” (Fig. 4). The slow scenario of model CTL underestimates mesopelagic (0– \approx 2000 m) phosphate in the North Pacific, and overestimates its concentration in the deep waters of this region (Fig. 4, panel A1). Increasing transport of organic matter to the deep ocean, as in scenario “fast” (panel A2 of Fig. 4) further reduces shallow and mesopelagic, and increases deep (> 2000 m) phosphate in this region. At the same time, phosphate in the North Atlantic is reduced. Therefore, in accordance with Kriest et al. (2012), increasing the remineralization length scale in model CTL has the effect of shifting nutrients downwards, and towards older waters along the “conveyor belt”. Introducing burial in model BUR leads to “slow” and “fast” model solutions that are more similar to each other than the corresponding solutions of model CTL. Introducing burial has little effect on shallow and mesopelagic nutrients in both scenarios “slow” and “fast”, but reduces deep nutrients in the northern North Pacific of the “fast” scenario making them more similar to those of the “slow” scenario (panels A3 and A4 of Fig. 4).

Burial thus lowers the sensitivity of deep model nutrients to changes in remineralization length scale. Likewise, the sensitivity of simulated deep phosphate in the Eastern Equatorial Pacific (EEP) to changes in sinking speed is reduced, as evident in Fig. 5, panels A1 to A4. As a consequence, the models’ misfit to observed phosphate (calculated as global average of the root-mean-square error RMSE; see also Kriest et al., 2010) becomes less sensitive to the remineralization length scale when introducing burial (Fig. 6). Instantaneous remineralization of organic matter at the sea floor (as introduced in model “INST”) shows almost the same distribution and sensitivity of phosphate and oxygen as in model CTL (see Figs. 6 and 7).

Interestingly, the impact of burial on the oxygen distribution is even more pronounced than its impact on phosphate. While the fast scenario of model CTL shows a severe

BGD

10, 10859–10911, 2013

Organic matter burial in global biogeochemical ocean models

I. Kriest and A. Oschlies

Title Page

Abstract

Introduction

Conclusions

References

Tables

Figures



Back

Close

Full Screen / Esc

Printer-friendly Version

Interactive Discussion

underestimate of simulated oxygen in the deep North Pacific and in the EEP, this underestimate almost disappears with the introduction of burial. Burial also considerably improves the deep oxygen in the EEP and in the northern North Pacific of the fast scenario. This is also evident from the volume distributions of oxygen for the different models: in contrast to that of phosphate, which is very similar among the different models and scenarios, oxygen distributions change considerably among the burial and non-burial models (Fig. 7). While scenario “fast” of model CTL predicts a far too large volume of water with low ($< \approx 100 \text{ mmol m}^{-3}$) oxygen, the detrimental effect of fast sinking disappears almost entirely when burial is considered (BUR). If burial is only weakly related to sediment input (WBUR), simulated oxygen again becomes more sensitive (compared to scenario BUR) to changes in the remineralization length scale. The lower sensitivity of simulated oxygen to changes in the remineralization length scale in model BUR is also evident from plots of the model misfit to oxygen vs. flux exponent (Fig. 6).

To summarize, adding burial yields a strong improvement of the modeled pelagic biogeochemical tracers at low flux exponents (comparable to a long remineralization length scale, or deep penetration of flux). The effect is most pronounced in old waters such as in the northern North Pacific, or in the EEP. As a consequence, simulated dissolved tracers become less sensitive to changes in remineralization length scale, thereby reducing the potential of biogeochemical water-column data to constrain this parameter. Given this weak sensitivity of both nutrients and oxygen simulated by model BUR, we refer to the title of our paper and ask to what extent possible impacts of model deficiencies may be “hidden” in the sediment. In next subsection we therefore examine the potential of additional diagnostics of particle fluxes and benthic-pelagic coupling to identify such deficiencies and to better constrain the respective model parameters and parameterizations.

BGD

10, 10859–10911, 2013

Organic matter burial in global biogeochemical ocean models

I. Kriest and A. Oschlies

Title Page

Abstract

Introduction

Conclusions

References

Tables

Figures

⏪

⏩

◀

▶

Back

Close

Full Screen / Esc

Printer-friendly Version

Interactive Discussion

5 Particle flux in the water column and at the sediment–water interface

5.1 Particle flux in the water column

In Fig. 8 we compare the particle flux in 2000 m simulated by the different sinking scenarios of model BUR against observations compiled by Honjo et al. (2008). The models reflect the general pattern of high particle flux in the high northern latitudes and the upwelling regions, and low particle flux in the oligotrophic subtropical gyres. As expected, decreasing the flux exponent increases particle flux at 2000 m, especially in the eutrophic regions. Simulated global particle flux as well as its pattern is quite insensitive to changes in the strength of burial (see Table 2). The slow scenarios yield the lowest RMS misfit to observed flux of 112 and 113 $\text{mmolC m}^{-2} \text{yr}^{-1}$ for runs CTL and BUR, respectively (see Table 2). However, the moderate to fast settling scenarios of these models still overestimate particle flux in the Southern Ocean (see Fig. 8), particularly for the reference scenario.

5.2 Benthic remineralization

Because our models do not represent the sediment explicitly, defining the model's counterpart to observations of benthic remineralization is not straightforward. We may, however, approximate benthic remineralization using the following assumptions: Over long time scales every (simulated) detritus particle in the model's deepest grid box will have encountered the sediment at least once. Although the model's upstream scheme assumes that this resuspended detritus is equally distributed within the grid box, we may also view it as sediment “fluff”, i.e. as organic matter that is only loosely associated with the sediment, but can be easily remobilized by currents, animals, etc. We therefore define detritus remineralization vertically integrated over the deepest model box as an (upper) model estimate of benthic remineralization per sea-floor area.

Figure 9 shows simulated benthic remineralization of model BUR, together with observations as compiled by Seiter et al. (2005, we use a data set provided by Christian

Title Page

Abstract

Introduction

Conclusions

References

Tables

Figures

⏪

⏩

◀

▶

Back

Close

Full Screen / Esc

Printer-friendly Version

Interactive Discussion



Hensen). The data set is supplemented by observations of Fischer et al. (2009) taken in the South Pacific, an area which otherwise would be only sparsely represented in the observations. In general, the model scenarios reflect the very high benthic remineralization rates observed along the coasts, and predict very low remineralization in the subtropical gyres. For the Northern Hemisphere the simulated low subtropical values are supported only by the few observations by Seiter et al. (2005). However, in the South Pacific Fischer et al. (2009) observed some sites with rather high benthic fluxes, which are not simulated by the model.

Another severe model-observation mismatch can be found in the Arabian Sea. Here the observations suggest extremely high benthic fluxes, whereas the model predicts rather low benthic remineralization. As the sites in the Arabian Sea are quite far from continental slopes, lateral advection does not serve to explain the apparent mismatch. We note that the very high fluxes shown by five data points collected in the Arabian Sea cannot be simulated by any of our model experiments, and therefore strongly deteriorate the model's fit to observations. Because the observations in this region have been derived from a local model fit to observed sediment properties (Luff et al., 2000), and because the global z-level models often fail to represent the complex hydrodynamic and biogeochemical structures of the Arabian Sea (Kriest, unpubl.; Dietze, personal communication, 2013), we have skipped these observational estimates from model comparison.

The fit of the models with pronounced burial (BUR, DUNNE) to observations of benthic remineralization improves with faster settling speed (Table 2 and Fig. 9). This is in contrast to the fit to observations of the particle flux at 2000 m described above, which tends to be best for slow settling speeds. This can be ascribed to higher benthic remineralization with increasing flux to the ocean floor, as well as to a steeper gradient between regions of simulated low and high benthic fluxes. If burial is weaker, as in model WBUR, the misfit to observations of benthic respiration is larger (Table 2), with a minimum misfit at medium settling speed. Without burial (CTL), the faster sink-

Organic matter burial in global biogeochemical ocean models

I. Kriest and A. Oschlies

Title Page

Abstract

Introduction

Conclusions

References

Tables

Figures

⏪

⏩

◀

▶

Back

Close

Full Screen / Esc

Printer-friendly Version

Interactive Discussion



ing leads to an overestimate in benthic remineralization in many regions, resulting in a worse fit (Table 2).

5.3 Burial in the sediment

We compare simulated burial flux to the observations described in Appendix A, which provides more details about the individual data sets. As in both the model and the observations burial is defined by the fact, that organic matter is removed from the system for a very long time, the model-data comparison appears more straightforward than for benthic remineralization.

When simulating medium to fast settling speed, model BUR often overestimates observed burial (Fig. 10), except for the coastal regions off Washington, California and Mexico. The overestimate is most severe in the EEP. In addition, slow sinking together with the insufficient representation of shelf regions leads to a quite low simulated burial of organic matter off California and Washington, and therefore to an increase of the RMS misfit. Therefore, although simulated burial mitigates the otherwise too high oxygen consumption by remineralization in the EEP under medium to fast settling speed, it results in unrealistically high burial of organic matter below the sediment surface especially in this region. Compared to models with weak (WBUR) or – not surprisingly – no (CTL) burial, models BUR and DUNNE are in better RMS agreement with observed estimates of global burial (Table 2).

5.4 Global fluxes

Despite the sometimes considerable model-data mismatches in various regions, some of the models perform quite well when compared to global fluxes of organic matter (Table 2). Benthic and riverine fluxes in all models increase with decreasing flux exponent (= increasing particle settling speed). The strength of burial has only little influence on particle flux in 2000 m, but, as could be expected, global burial and therefore riverine

BGD

10, 10859–10911, 2013

Organic matter burial in global biogeochemical ocean models

I. Kriest and A. Oschlies

Title Page

Abstract

Introduction

Conclusions

References

Tables

Figures

⏪

⏩

◀

▶

Back

Close

Full Screen / Esc

Printer-friendly Version

Interactive Discussion

input is higher in models with strong burial (BUR and DUNNE), while benthic remineralization is higher in the model with weak burial (WBUR).

Despite the relatively fine ($1^\circ \times 1^\circ$) spatial resolution, the models do not resolve the shelf very well. This is reflected in a smaller difference between total and deep (> 2000 m) simulated benthic remineralization and burial than found in the observations. While the models simulate 40–66 % of total benthic remineralization, and 32–80 % of total burial to occur below 2000 m, observations suggest lower percentages for the “open ocean” (i.e. shelf and slope region omitted), of 26 and 29 % for remineralization and burial, respectively. Because of this deficient representation of coastal and shelf areas, in the following we focus on the deep (< 2000 m) fluxes.

Global particle flux in the water column at 2000 m depth is relatively insensitive to the implementation of burial, thus all models show about the same response to changes in particle sinking speed. Particle flux at 2000 m is reproduced best with slow settling speed (scenarios “very slow” and “slow”), a finding that agrees with results obtained with a coarser resolution of this model (see Kriest et al., 2012).

The implementation of burial, of course, has a strong impact on the model's representation of global burial at the sea floor. Model WBUR and, of course, models CTL and INST, underestimate global burial. At the same time, these models for moderate to fast sinking speeds overestimate benthic remineralization. Taken together, this points towards too weak burial, or too strong “resuspension” and subsequent remineralization in these models. In contrast, the base scenarios of BUR and DUNNE match observed global burial flux much better, but underestimate benthic remineralization. The sinking speed plays a strong role for these models' agreement with observed fluxes of burial.

BGD

10, 10859–10911, 2013

Organic matter burial in global biogeochemical ocean models

I. Kriest and A. Oschlies

[Title Page](#)

[Abstract](#)

[Introduction](#)

[Conclusions](#)

[References](#)

[Tables](#)

[Figures](#)

[⏪](#)

[⏩](#)

[◀](#)

[▶](#)

[Back](#)

[Close](#)

[Full Screen / Esc](#)

[Printer-friendly Version](#)

[Interactive Discussion](#)

6 Discussion

6.1 Sensitivity of dissolved tracers to particle flux and pelagic-benthic coupling

A finding that is, at first sight, surprising for a model with fixed stoichiometric relations is that simulated oxygen seems to be much more affected by changes in model structure and sinking speed than phosphate. The reason for the lower sensitivity of phosphate may be found in the fixed P-inventory imposed onto the model: although an increase in particle sinking speed will result in higher phosphate concentration in deeper and older waters, at the same time this increase is limited by the concomitant phosphate decrease in younger waters (see also Kriest et al., 2012). Thus, the misrepresentation of phosphate in the model is limited by the constraint of phosphorus mass conservation. In contrast, the oxygen inventory can change due to the combined effects of biogeochemistry, circulation and mixing, and air-sea gas exchange with the atmosphere, so that the model cannot only fail in the internal distribution of oxygen, but also in its average concentration.

The introduction of burial reduces the sensitivity especially of simulated oxygen distribution to changes in the particle flux exponent. The models with fast particle sinking now perform much better with respect to oxygen, the reason being most likely, that now “excess” organic matter, whose remineralization would strongly decrease oxygen, is buried in the sediment. In other words, it is “swept under the carpet”, and only reappears as phosphate in regions far away from the areas of burial. (Note that many of the world's major rivers discharge into the Atlantic Ocean; see Fig. 13.)

This reduced sensitivity of simulated dissolved tracers in the burial models poses problems for any method that aims at constraining the model parameters via calibration against global pelagic tracer distributions. A potential solution to this problem could be to use additional observations, such as pelagic and benthic fluxes of organic matter, that are more closely related to particle flux and remineralization. However, some peculiarities like mismatches in the spatial and temporal scales, and methodological

BGD

10, 10859–10911, 2013

Organic matter burial in global biogeochemical ocean models

I. Kriest and A. Oschlies

Title Page

Abstract

Introduction

Conclusions

References

Tables

Figures

⏪

⏩

◀

▶

Back

Close

Full Screen / Esc

Printer-friendly Version

Interactive Discussion

constraints can make such a direct comparison between models and observations difficult.

6.2 Comparison to vertical fluxes

It is beyond the scope of this paper to discuss the methodological problems associated with sediment traps (but see, e.g. Honjo et al., 2008, and citations therein). However, even with a perfect particle interceptor trap we would still have to deal with the spatial hydrographic variability around many trap locations, which may hinder a direct model-data comparison in regions of strong horizontal gradients (e.g. Siegel et al., 2008). On the other hand, the general overestimate of particle flux by the fast-settling models as evident in Fig. 8 indicates – together with the other metrics – that these are less likely to represent pelagic biogeochemical processes well (see also Kriest et al., 2012, for the relation between fit to estimated global flux and dissolved tracer).

Benthic C-org remineralization or dissolved oxygen utilization (“DOU”) is measured either (a) from pore water profiles and diffusion models, or (b) via the oxygen decline over time in benthic chambers. While method (a) can lead to decompression and handling artifacts, (b) can cause artifacts through benthic fauna activities (e.g. Glud et al., 1994). Further, while (a) represents a steady state system (due to the intrinsic assumptions), the benthic chamber used in (b) represents a snapshot of sediment respiration in an isolated system that excludes both transfer of organic matter to the sediment, as well as exchange with the surrounding water and dissolved oxygen. However, assuming that during the incubation time of typically a few days, the rate of respiration is neither carbon nor oxygen limited, this observation may well represent a steady state system.

Burial is usually estimated directly from ^{14}C age, mass accumulation rate and % C_{org} of the sediment cores. Comparing simulated and observed burial seems to be fairly straightforward, as both fluxes are defined by the fact that they are lost from the local system (water column + “active” sediment) for a very long time. Unfortunately, as we have seen above (Fig. 10) these observations are very sparse, and somehow

Organic matter burial in global biogeochemical ocean models

I. Kriest and A. Oschlies

Title Page

Abstract

Introduction

Conclusions

References

Tables

Figures

⏪

⏩

◀

▶

Back

Close

Full Screen / Esc

Printer-friendly Version

Interactive Discussion



biased towards coastal areas and/or highly productive regions. In addition, there may be complications and artifacts due to sediment focusing (e.g. Kienast et al., 2007), or potential age offsets among different sediment weight fractions (Heinze et al., 2009, and citations therein).

Overall, the spatial sparsity of the flux observations, their potential bias towards certain regions, as well as the sometimes difficult assignment of proper model counterparts to the observations make it difficult to use them as strong constraints on model performance. However, the models' overestimate of simulated burial especially under medium-to-high sinking rates in the eastern equatorial Pacific (EEP) points towards a potential lack or misrepresentation of processes by the models in that region. We thus regard the flux observations as useful additional model constraint, that may complement any model assessment based on more "traditional" observations such as nutrients or oxygen.

6.3 Model performance in the Eastern Equatorial Pacific and in coastal areas

A potential explanation for the apparent misfits in the EEP could be the neglect of oxygen sensitivity of remineralization in the model. This neglect currently allows for complete consumption of oxygen at unaltered remineralization rates, whenever the supply of organic matter is high enough. Thereby the current model assumes a form of "implicit" denitrification, as remineralization continues even in the absence of oxygen. In a future study we will investigate the impact of this assumption on the model-data misfits particularly in the EEP, and examine whether the implementation of nitrate as additional oxidant ameliorates this model-data mismatch.

An alternative explanation for the mismatches in the EEP could be a misrepresentation of the Equatorial Intermediate Current System in this region, resulting in too low oxygen (Dietze and Loeptien, 2013). According to that study, and citations therein, the problem is "endemic even to eddy-resolving circulation models". Improved representations of physical processes in regional or nested global models might help to resolve this problem.

Organic matter burial in global biogeochemical ocean models

I. Kriest and A. Oschlies

Title Page

Abstract

Introduction

Conclusions

References

Tables

Figures



Back

Close

Full Screen / Esc

Printer-friendly Version

Interactive Discussion



Organic matter burial in global biogeochemical ocean models

I. Kriest and A. Oschlies

[Title Page](#)

[Abstract](#)

[Introduction](#)

[Conclusions](#)

[References](#)

[Tables](#)

[Figures](#)

[⏪](#)

[⏩](#)

[◀](#)

[▶](#)

[Back](#)

[Close](#)

[Full Screen / Esc](#)

[Printer-friendly Version](#)

[Interactive Discussion](#)



When neglecting shelf areas, the models with strong burial seem to be better suited to represent global vertical fluxes, although results for particle flux at 2000 m, benthic remineralization and burial point towards different “best” candidates. It remains to be investigated, whether a better topographic representation of coastal and shelf areas helps to achieve a closer match to local observations of benthic processes, as well as to global estimates of sediment-water exchange.

6.4 Combining model metrics

So far it seems that the addition of burial has been of little benefit to the model in terms of its ability to reproduce water-column distributions of biogeochemical tracers. A main effect of burial in the model is a weakening of the constraints provided by water-column tracer distributions on the remineralization length scale, thereby making the model more robust with respect to errors in the parameterization of particle flux. At moderate to slow sinking speeds all models represent dissolved tracers about equally well.

In order to identify a “best” model type, we have evaluated model performance using a combined metric of dissolved tracers and vertical fluxes. The metric consists of terms for normalized root-mean-square-errors (RMSE) for phosphate (r_P), oxygen (r_O), particle flux (r_F), benthic remineralization (r_R) and burial (r_B). We further complemented the analysis of model skill by calculating the relative deviation of simulated to observed global oxygen inventory (d_O ; expressed as global average oxygen) as well as simulated to observed global particle flux (d_F), benthic remineralization (d_R), burial (d_B) and river runoff (d_r). (As noted above, because of mass conservation, the global phosphate inventory does not help to constrain the model, and is therefore not used for model assessment.) To add quantities of different units, we have normalized the RMSE and deviations of oxygen by the respective observed average global concentration. RMSE and deviations of vertical fluxes have been normalized by the respective global fluxes

Summarizing, despite too high burial rates in certain regions, we regard models BUR or DUNNE as more suitable than CTL or INST without any pelagic-benthic coupling, or model WBUR with only weak burial at the seafloor.

6.5 Deep detritus: an “escape route” for excess organic matter?

5 So far, we have investigated dissolved tracers in the water column, as well as vertical and benthic fluxes. What remains is to examine the last potential “escape route” for excess organic matter that sinks to the sea floor, namely detritus in the deep ocean.

In models BUR and DUNNE we allowed particulate organic matter to be locked away in the sediment, thereby mimicking burial and/or the activity of benthic organisms. Possible alternatives – in particular the instantaneous remineralization of sedimenting organic matter – would imply an extremely active benthic fauna, and further result in too high nutrient concentrations (and too low oxygen concentrations) in the bottom water under certain settling scenarios. The “reflection” of organic matter, in conjunction with benthic burial, on the other hand, results in more reasonable nutrient and oxygen concentrations over a wider range of sinking exponents (Fig. 3).

The lower phosphate and higher oxygen concentrations in the bottom box of the two “best” models DUNNE and BUR come not only at the cost of partly too high burial, but are also accompanied by elevated deep detritus concentrations. However, we argue that these are not unrealistically high. While model INST due to its inherent assumptions shows decreasing detritus concentrations with depth (Fig. 12), model CTL exhibits elevated (in contrast to the layer above) detritus at the sea floor. In some areas detritus increases towards the seafloor even more than 10-fold (Fig. 12). Burial reduces this increase towards values that are four to seven times that of the overlying layer, thereby mimicking a benthic nepheloid layer (“BNL”).

25 BNLs are indicated by elevated turbidity and have been observed in many different regions (Vangriesheim et al., 2001; Inthorn et al., 2006; Lukashin and Shcherbinin, 2007; Capello et al., 2009; Fischer et al., 2009). Typically, the BNL has a thickness up to tens to hundreds of meters (e.g. Turnewitsch and Springer, 2001; Inthorn et al.,

Organic matter burial in global biogeochemical ocean models

I. Kriest and A. Oschlies

Title Page

Abstract

Introduction

Conclusions

References

Tables

Figures



Back

Close

Full Screen / Esc

Printer-friendly Version

Interactive Discussion



2006). The amount and spatial extension of these remobilizations depends not only on physical processes, but also on the megafauna composition, the type of the material deposited (e.g. Vangriesheim et al., 2001; Lampitt et al., 2001), or the abundance and activity of groundfish (Yahel et al., 2008).

5 The large relative increase of detritus in in the bottom box compared to the overlying grid box exhibited by model CTL seems to be rather high when compared to observations, but model BUR with its less pronounced particle increase seems to be more in line with observations of a several fold increase of particle number or mass taken e.g by Boetius et al. (2000); McCave et al. (2001) or Lukashin and Shcherbinin (2007).
10 The relative increase of detritus in the bottom layer, compared to the layer above, declines with slower sinking speed (no figure), and increases with faster sinking speed, particularly for model CTL. Thus, differences between CTL and BUR decrease for slow sinking speeds.

As shown above, some scenarios of models BUR and DUNNE perform best with respect to a combined metric of dissolved tracers and fluxes. By avoiding extreme tracer concentrations near the seafloor, they might therefore serve as a good starting point for a later parameterization of oxidant sensitive processes such as oxygen dependent remineralization or denitrification.

7 Conclusions

20 In contrast to the constraint of mass conservation imposed on phosphorus, exchange of oxygen with the atmosphere results in variable oxygen inventory. Therefore, simulated oxygen is more affected by changes in model structure and sinking speed than phosphate. The introduction of burial reduces the sensitivity of simulated oxygen and, to a lesser extent, phosphate distributions to changes in the particle flux. In some regions remineralization of (sinking) organic matter would cause a severe oxygen deficit.
25 In models that allow burial in the sediment, this (problem) is “swept under the carpet”.

Organic matter burial in global biogeochemical ocean models

I. Kriest and A. Oschlies

Title Page

Abstract

Introduction

Conclusions

References

Tables

Figures

◀

▶

◀

▶

Back

Close

Full Screen / Esc

Printer-friendly Version

Interactive Discussion



transformed data between “net sediment accumulation” and “burial” (burial calculated from burial efficiency times net sediment accumulation). This gives $\alpha = 0.9345$ and $\beta = 1.6542$, with $r^2 = 0.97$ (see also Fig. 1). We note that burial efficiencies estimated from low bottom water oxygen sediments are just slightly slightly enhanced; sediment accumulation seems to play a much larger role for burial efficiency.

Many of the data sources in Burdige’s data set give burial and carbon rain rate (Lohse et al., 1998; Sayles et al., 2001; Stahl et al., 2004, e.g.). Regarding the data set by Hartnett and Devol (2003), we found it difficult to extract the exact station location from their description. We therefore in the following refer to the data set by Devol and Hartnett (2001) for the continental margin off Washington State and Mexico. Some of Burdige’s data points are taken from the data set by Canfield (1994). This data set, among others, uses the data from the following sources: Bender and Heggie (1984, NE Pacific and equatorial Atlantic), Berelson et al. (1987, Californian Borderland – S. Pedro and S. Nicolas), Bender et al. (1989, Californian Borderland – S. Clemente), Jahnke et al. (1990, Californian Borderland – S. Monica and S. Catalina; note that Canfield only uses the data for station S. Pedro from the this dataset). Other data sources are for Danish coastal waters, Baltic Sea, coastal North Carolina, Long Island Sound, etc. (i.e., mainly coastal waters), or for enclosed anoxic basins and seas such as the Cariaco Trench or the Black Sea. Omitting the coastal and anoxic regions from the analysis, we are therefore left with eight data sets from Burdige’s compilation.

A2 Our data compilation

In addition to the eight data sets named above, we have further added the data set by Berelson et al. (1997), which gives burial and remineralization rates for the equatorial Pacific along 140° W. The data set by Kienast et al. (2007) only gives burial rates for the Panama Basin. As this region is especially sensitive to ventilation and biogeochemical parameters (especially DOP decay parameters; see Kwon and Primeau, 2006), we have added this data set as a valuable constraint on simulated burial. We supplemented it by carbon rain rate to the sea floor, derived from sediment traps deployed

Organic matter burial in global biogeochemical ocean models

I. Kriest and A. Oschlies

Title Page

Abstract

Introduction

Conclusions

References

Tables

Figures

⏪

⏩

◀

▶

Back

Close

Full Screen / Esc

Printer-friendly Version

Interactive Discussion



in the vicinity of this site (Honjo et al., 1992). Taken together, we therefore have 10 different data sets:

1. Bender and Heggie (1984) – Pacific and Atlantic: We used their Table 12 and station locations from their Table 1. For the site in the eastern equatorial Atlantic we only considered the five stations nearest the equator. We only considered C_{org} -oxidation from O_2 .
2. Berelson et al. (1987) – Californian Borderland (S. Pedro and S. Nicolas): We used their Table 8 for remineralization and burial rate of C_{org} . Station locations were determined from their Fig. 1, and station depths from their Table 1.
3. Bender et al. (1989) – Californian Borderland (S. Clemente): We used C_{org} fluxes from their Fig. 10. Station locations were calculated from averages of all stations listed in their Table 1.
4. Jahnke et al. (1990) – Californian Borderland (S. Monica and S. Catalina): We used Table 3 from Jahnke et al. (1990), but only values for S. Catalina and S. Monica. Station locations were read from their Fig. 1. For depth we used the value of the nearest isoline.
5. Berelson et al. (1997) – Equatorial Pacific: Station locations and fluxes were taken from their Table 1, but only for stations where all fluxes (rain rate, remineralization and burial rate) are available. If there is more than one value, we calculated the average.
6. Lohse et al. (1998) – OMEX: We used Table 6 of Lohse et al. (1998), averaged over regions “shelf” (A), “upper slope” (I, B, II), “lower slope” (C, F, III) and PAP (E). Station locations, listed in Table 1, were averaged accordingly.
7. Sayles et al. (2001) – Ross Sea: Averages of station locations were taken from Table 1. Fluxes were extracted from Table 12. For remineralization we used the

Organic matter burial in global biogeochemical ocean models

I. Kriest and A. Oschlies

Title Page

Abstract

Introduction

Conclusions

References

Tables

Figures



Back

Close

Full Screen / Esc

Printer-friendly Version

Interactive Discussion



“NO₃⁻ Remin” value. For a range of fluxes, we took the average (center) of this value. For burial, we used the first (²³⁰Th-normalized) rate.

8. Devol and Hartnett (2001) – off Washington and Mexico: Table 1 from Devol and Hartnett (2001) contains 22 entries. We used averages over $i = 1 : 13$ for the region off Washington State, and for $i = 14 : 22$ for the region off Mexico, for location, depth and fluxes of rain rate, burial and remineralization.
9. Stahl et al. (2004) – Porcupine Abyssal Plain (PAP): We read flux for station PAP from their Fig. 6. Station location was taken from their Table 1 (average over all values).
10. Kienast et al. (2007) and Honjo et al. (1992) – Panama Basin: Burial data (Acc. rate) were read from Fig. 8, carbon flux from mass accumulation rate. Station locations were taken from their Table 1. For core P7, we have added the trap-derived sedimentation rate of $10.87 \text{ mg C m}^{-2} \text{ d}^{-1}$ at 2869 m observed by Honjo et al. (1992, their Table 5; “Honjo – A”). Note that this value is probably an upper estimate of the carbon rain rate to the sea floor, in the vicinity of this site.

Table 4 shows the fluxes converted to $\text{mmol C m}^{-2} \text{ yr}^{-1}$. For the plot shown in Fig. 1 and corresponding regressions, we used remineralization + burial as total flux to the sea floor. In case where there was no remineralization available (data by Kienast et al., 2007 and Lohse et al., 1998) we used the rain rate to the sediment as upper estimate for remineralization rate. Note that in these two data sets, burial is just a small fraction of rain rate – therefore, subtracting it from the rain rate would have made only a small difference to the regression.

Appendix B

Data set for river runoff

We use the data set of volumetric flow rates given in Perry et al. (1996). Because little seems to be known about their nutrient contents of Arctic rivers (but see the recent paper by Holmes et al., 2012), and because during model simulation the nutrient supply via these rivers may get trapped in the Arctic, we excluded the 14 rivers that discharge north of 60° N, namely Yenisei, Lena, Ob, MacKenzie, Yukon, Pechora, Severnaya Dvina, Khatanga-Popigay, Kolyma, Pyasina, Indigirka, Taz, Kuskokwim, and Copper. For the remaining 61 rivers, we calculated the minimum distance of their mouth's location to the corresponding model location in the MIT2.8 configuration. We only included rivers which have a corresponding "wet" point in the model within a distance of two times the model grid resolution (2.8°), times $\sqrt{2}$. Because the MIT2.8 model does not resolve many marginal seas, this results in the omission of the following rivers from the data set: Danube, Dniepr (Black Sea); Nile, Po, Rhone (Mediterranean Sea); Nelson, La Grande (Hudson Bay); Neva (Baltic Sea); Shatt al-Arab (Persian Gulf); Huang Ho (Yellow Sea).

In order to account for the potentially large fan of river runoff, we first calculated the number of all surface model boxes that are influenced by a river in the modified data set. In case a river discharge exceeds half of the corresponding model surface box volume per year, we extended the region over which this discharge is distributed equally over several surface boxes. In the MIT2.8 model geometry this only affects the Amazon outflow, whose discharge is being distributed over 11 horizontal grid points around its mouth. The resulting runoff (discharge volume of a river, expressed as fraction of total discharge of all rivers), and all river locations south of 60° N from the original data set are shown in Fig. 13.

For the parameterization of runoff fields for ECCO, we use the MIT2.8 runoff volumes, remapped onto the ECCO geometry. By doing so, we assure that the riverine input

BGD

10, 10859–10911, 2013

Organic matter burial in global biogeochemical ocean models

I. Kriest and A. Oschlies

Title Page

Abstract

Introduction

Conclusions

References

Tables

Figures

⏪

⏩

◀

▶

Back

Close

Full Screen / Esc

Printer-friendly Version

Interactive Discussion



of buried P happens at approximately the same location in both model configurations. Burial and runoff for both model types show about the same magnitude and distribution, with some difference along the coasts. Although not shown here, the general response of the MIT2.8 model to the introduction of burial and runoff is the same.

5 *Acknowledgements.* This work is a contribution to the DFG-supported project SFB754. We acknowledge financial support from the EU FP7 project CARBOCHANGE (grant agreement no. 264879). Parallel supercomputing resources have been provided by the North-German Supercomputing Alliance (HLRN). The authors wish to acknowledge use of the Ferret program of NOAA's Pacific Marine Environmental Laboratory for analysis and graphics in this paper.

10

The service charges for this open access publication have been covered by a Research Centre of the Helmholtz Association.

References

15

Aumont, O. and Bopp, L.: Globalizing results from ocean in situ iron fertilization studies, *Global Biogeochem. Cy.*, 20, GB2017, doi:10.1029/2005GB002591, 2006. 10861, 10863

Bacon, M. P. and van der Loeff, M. M. R.: Removal of Th-234 by scavenging in the bottom nepheloid layer of the ocean, *Earth Planet. Sc. Lett.*, 92, 157–164, doi:10.1016/0012-821X(89)90043-5, 1989. 10865

20

Bender, M. L. and Heggie, D. T.: Fate of organic carbon reaching the deep sea floor: a status report, *Geochim. Cosmochim. Ac.*, 48, 977–986, 1984. 10884, 10885

Bender, M., Jahnke, R., Weiss, R., Martin, W., Heggie, D. T., Orchardo, J., and Sowers, T.: Organic-carbon oxidation and benthic nitrogen and silica dynamics in San-Clemente Basin, a continental borderland site, *Geochim. Cosmochim. Ac.*, 53, 685–697, doi:10.1016/0016-7037(89)90011-2, 1989. 10884, 10885

25

Berelson, W. M., Hammond, D. E., and Johnson, K. S.: Benthic fluxes and the cycling of biogenic silica and carbon in two southern-california borderland basins, *Geochim. Cosmochim. Ac.*, 51, 1345–1363, doi:10.1016/0016-7037(87)90320-6, 1987. 10884, 10885

Organic matter burial in global biogeochemical ocean models

I. Kriest and A. Oschlies

[Title Page](#)
[Abstract](#)
[Introduction](#)
[Conclusions](#)
[References](#)
[Tables](#)
[Figures](#)




[Back](#)
[Close](#)
[Full Screen / Esc](#)
[Printer-friendly Version](#)
[Interactive Discussion](#)


- Berelson, W., Anderson, R., Dymond, J., Demaster, D., Hammond, D., Collier, R., Honjo, S., Leinen, M., Mcmanus, J., Pope, R., Smith, C., and Stephens, M.: Biogenic budgets of particle rain, benthic remineralization and sediment accumulation in the equatorial Pacific, *Deep-Sea Res. Pt. II*, 44, 2251–2282, doi:10.1016/S0967-0645(97)00030-1, 1997. 10884, 10885
- 5 Bianchi, D., Galbraith, E. D., Carozza, D. A., Mislán, K. A. S., and Stock, C. A.: Intensification of open-ocean oxygen depletion by vertically migrating animals, *Nat. Geosci.*, 6, 545–548, doi:10.1038/NGEO1837, 2013. 10861
- Boetius, A., Springer, B., and Petry, C.: Microbial activity and particulate matter in the benthic nepheloid layer (BNL) of the deep Arabian Sea, *Deep-Sea Res. Pt. II*, 47, 2687–2706, 2000. 10882
- 10 Burdige, D. J.: Preservation of organic matter in marine sediments: controls, mechanisms, and an imbalance in sediment organic carbon budgets?, *Chem. Rev.*, 107, 467–485, 2007. 10863, 10864, 10883, 10899
- Canfield, D. E.: Factors influencing organic carbon preservation in marine sediments, *Chem. Geol.*, 114, 315–329, doi:10.1016/0009-2541(94)90061-2, 1994. 10884
- 15 Capello, M., Budillon, G., Cutroneo, L., and Tucci, S.: The nepheloid bottom layer and water masses at the shelf break of the western Ross Sea, *Deep-Sea Res. Pt. II*, 56, 843–858, doi:10.1016/j.dsr2.2008.10.032, 2009. 10881
- Devol, A. H. and Hartnett, H. E.: Role of the oxygen-deficient zone in transfer of organic carbon to the deep ocean, *Limnol. Oceanogr.*, 46, 1684–1690, 2001. 10884, 10886
- 20 Dietze, H. and Loeptien, U.: Revisiting “nutrient trapping” in global coupled biogeochemical ocean circulation models, *Global Biogeochem. Cy.*, 27, 1–20, doi:10.1002/gbc.20029, 2013. 10878
- Dunne, J. P., Sarmiento, J. L., and Gnanadesikan, A.: A synthesis of global particle export from the surface ocean and cycling through the ocean interior and on the seafloor, *Global Biogeochem. Cy.*, 21, GB4006, doi:10.1029/2006GB002907, 2007. 10864, 10867, 10895, 10899
- 25 Duteil, O. and Oschlies, A.: Sensitivity of simulated extent and future evolution of marine suboxia to mixing intensity, *Geophys. Res. Lett.*, 38, L06607, doi:10.1029/2011GL046877, 2011. 10861
- 30 Fischer, J. P., Ferdelman, T. G., D’Hondt, S., Røy, H., and Wenzhöfer, F.: Oxygen penetration deep into the sediment of the South Pacific gyre, *Biogeosciences*, 6, 1467–1478, doi:10.5194/bg-6-1467-2009, 2009. 10873, 10881, 10907

**Organic matter burial
in global
biogeochemical
ocean models**

I. Kriest and A. Oschlies

Title Page

Abstract

Introduction

Conclusions

References

Tables

Figures

◀

▶

◀

▶

Back

Close

Full Screen / Esc

Printer-friendly Version

Interactive Discussion



Flögel, S., Wallmann, K., Poulsen, C. J., Zhou, J., Oschlies, A., Voigt, S., and Kuhnt, W.: Simulating the biogeochemical effects of volcanic CO₂ degassing on the oxygen-state of the deep ocean during the Cenomanian/Turonian Anoxic Event (OAE2), *Earth Planet. Sci. Lett.*, 305, 371–384, doi:10.1016/j.epsl.2011.03.018, 2011. 10864, 10899

5 Garcia, H. E., Locarnini, R. A., Boyer, T. P., and Antonov, J. I.: World Ocean Atlas 2005, Vol. 4: Nutrients (phosphate, nitrate, silicate), in: NOAA Atlas NESDIS 64, edited by: Levitus, S., US Government Printing Office, Washington, DC, available at: <http://iridl.Ideo.columbia.edu/SOURCES/.NOAA/.NODC/.WOA05/>, 2006a. 10867, 10901

10 Garcia, H. E., Locarnini, R. A., Boyer, T. P., and Antonov, J. I.: World Ocean Atlas 2005, vol. 3: Dissolved oxygen, apparent oxygen utilization, and oxygen saturation, in: NOAA Atlas NESDIS 63, edited by: Levitus, S., US Government Printing Office, Washington, DC, available at: <http://iridl.Ideo.columbia.edu/SOURCES/.NOAA/.NODC/.WOA05/>, 2006b. 10867, 10901

15 Glud, R. N., Gundersen, J. K., Jorgensen, B. B., Revsbech, N. P., and Schulz, H. D.: Diffusive and total oxygen uptake of deep-sea sediments in the eastern south atlantic ocean: in situ and laboratory measurements, *Deep-Sea Res. Pt. I*, 41, 1767–1788, 1994. 10877

Hartnett, H. E. and Devol, A. H.: Role of a strong oxygen-deficient zone in the preservation and degradation of organic matter: a carbon budget for the continental margins of northwest Mexico and Washington State, *Geochim. Cosmochim. Ac.*, 67, 247–264, doi:10.1016/S0016-7037(02)01076-1, 2003. 10884

20 Heinze, C., Kriest, I., and Maier-Reimer, E.: Age offsets among different biogenic and lithogenic components of sediment cores revealed by numerical modeling, *Paleoceanography*, 24, PA4214, doi:10.1029/2008PA001662, 2009. 10878

Holmes, R. M., McClelland, J. W., Peterson, B. J., Tank, S. E., Bulygina, E., Eglinton, T. I., Gordeev, V. V., Gurtovaya, T. Y., Raymond, P. A., Repeta, D. J., Staples, R., Striegl, R. G., Zhulidov, A. V., and Zimov, S. A.: Seasonal and annual fluxes of nutrients and organic matter from large rivers to the Arctic Ocean and surrounding seas, *Estuar. Coast.*, 35, 369–382, doi:10.1007/s12237-011-9386-6, 2012. 10887

Honjo, S., Spencer, D., and Gardner, W.: A sediment trap intercomparison experiment in the Panama Basin, 1979, *Deep-Sea Res. Pt. I*, 39, 333–358, 1992. 10885, 10886, 10898

30 Honjo, S., Manganini, S. J., Krishfield, R. A., and Francois, R.: Particulate organic carbon fluxes to the ocean interior and factors controlling the biological pump: A synthesis of global sediment trap programs since 1983, *Prog. Oceanogr.*, 76, 217–285, doi:10.1016/j.pocean.2007.11.003, 2008. 10872, 10877, 10896, 10906

Organic matter burial in global biogeochemical ocean models

I. Kriest and A. Oschlies

[Title Page](#)
[Abstract](#)
[Introduction](#)
[Conclusions](#)
[References](#)
[Tables](#)
[Figures](#)




[Back](#)
[Close](#)
[Full Screen / Esc](#)
[Printer-friendly Version](#)
[Interactive Discussion](#)

Inthorn, M., Mohrholz, V., and Zabel, M.: Nepheloid layer distribution in the Benguela upwelling area offshore Namibia, *Deep-Sea Res. Pt. I*, 53, 1423–1438, doi:10.1016/j.dsr.2006.06.004, 2006. 10881

Jahnke, R. A., Reimers, C. E., and Craven, D. B.: Intensification of recycling of organic matter at the sea floor near ocean margins, *Nature*, 348, 1990. 10884, 10885

Khatiwala, S.: A computational framework for simulation of biogeochemical tracers in the ocean, *Global Biogeochem. Cy.*, 21, GB3001, doi:10.1029/2007GB002923, 2007. 10862

Khatiwala, S., Visbeck, M., and Cane, M. A.: Accelerated simulation of passive tracers in ocean circulation models, *Ocean Modell.*, 9, 51–69, 2005. 10862

Kienast, S. S., Kienast, M., Mix, A. C., Calvert, S. E., and Francois, R.: Thorium-230 normalized particle flux and sediment focusing in the Panama Basin region during the last 30 000 years, *Paleoceanography*, 22, PA2213, doi:10.1029/2006PA001357, 2007. 10878, 10884, 10886

Kriest, I. and Oschlies, A.: Numerical effects on organic matter sedimentation and remineralization in biogeochemical ocean models, *Ocean Modell.*, 39, 275–283, doi:10.1016/j.ocemod.2011.05.001, 2011. 10868, 10869

Kriest, I., Khatiwala, S., and Oschlies, A.: Towards an assessment of simple global marine biogeochemical models of different complexity, *Prog. Oceanogr.*, 86, 337–360, doi:10.1016/j.pocean.2010.05.002, 2010. 10862, 10863, 10870

Kriest, I., Oschlies, A., and Khatiwala, S.: Sensitivity analysis of simple global marine biogeochemical models, *Global Biogeochem. Cy.*, 26, GB2029, doi:10.1029/2011GB004072, 2012. 10862, 10863, 10866, 10869, 10870, 10875, 10876, 10877, 10880, 10895

Kwon, E. Y. and Primeau, F.: Optimization and sensitivity study of a biogeochemistry ocean model using an implicit solver and in situ phosphate data, *Global Biogeochem. Cy.*, 20, GB4009, doi:10.1029/2005GB002631, 2006. 10869, 10884

Lampitt, R. S., Bett, B. J., Kiriakoulakis, K., Popova, E. E., Ragueneau, O., Vangriesheim, A., and Wolff, G. A.: Material supply to the abyssal seafloor in the Northeast Atlantic, *Prog. Oceanogr.*, 50, 27–63, doi:10.1016/S0079-6611(01)00047-7, 2001. 10882

Lohse, L., Helder, W., Epping, E. H. G., and Balzer, W.: Recycling of organic matter along a shelf-slope transect across the N.W. European Continental Margin (Goban Spur), *Prog. Oceanogr.*, 42, 77–110, doi:10.1016/S0079-6611(98)00029-9, 1998. 10884, 10885, 10886

Luff, R., Wallmann, K., Grandel, S., and Schluter, M.: Numerical modeling of benthic processes in the deep Arabian Sea, *Deep-Sea Res. Pt. II*, 47, 3039–3072, doi:10.1016/S0967-0645(00)00058-8, 2000. 10873

Organic matter burial in global biogeochemical ocean models

I. Kriest and A. Oschlies

[Title Page](#)
[Abstract](#)
[Introduction](#)
[Conclusions](#)
[References](#)
[Tables](#)
[Figures](#)
[⏪](#)
[⏩](#)
[◀](#)
[▶](#)
[Back](#)
[Close](#)
[Full Screen / Esc](#)
[Printer-friendly Version](#)
[Interactive Discussion](#)

Lukashin, V. N. and Shcherbinin, A. D.: The nepheloid layer and horizontal sedimentary matter fluxes in the Norwegian Sea, *Oceanology*, 47, 833–847, doi:10.1134/S0001437007060082, 2007. 10881, 10882

Marchal, O., Stocker, T. F., and Joos, F.: A latitude-depth, circulation-biogeochemical ocean model for paleoclimate studies. Development and sensitivities, *Tellus B*, 50, 290–316, doi:10.1034/j.1600-0889.1998.t01-2-00006.x, 1998. 10862, 10863

Martin, J. H., Knauer, G. A., Karl, D. M., and Broenkow, W. W.: VERTEX: carbon cycling in the Northeast Pacific, *Deep-Sea Res.*, 34, 267–285, 1987. 10863

Matear, R. J., and Hirst, A. C.: Long-term changes in dissolved oxygen concentrations in the ocean caused by protracted global warming, *Global Biogeochem. Cy.*, 17, 1125, doi:10.1029/2002GB001997, 2003. 10861, 10862, 10863

McCave, I. N., Hall, I. R., Antia, A. N., Chou, L., Dehairs, F., Lampitt, R. S., Thomsen, L., van Weering, T. C. E., and Wollast, R.: Distribution, composition and flux of particulate material over the European margin at 47–50° N, *Deep-Sea Res. Pt. II*, 48, 3107–3139, 2001. 10882

Moore, J. K. and Doney, S. C.: Iron availability limits the ocean nitrogen inventory stabilizing feedbacks between marine denitrification and nitrogen fixation, *Global Biogeochem. Cy.*, 21, GB2001, doi:10.1029/2006GB002762, 2007.

Najjar, R. G., Jin, X., Louanchi, F., Aumont, O., Caldeira, K., Doney, S. C., Dutay, J.-C., Follows, M., Gruber, N., Joos, F., Lindsay, K., Maier-Reimer, E., Matear, R., Matsumoto, K., Monfray, P., Mouchet, A., Orr, J. C., Plattner, G.-K., Sarmiento, J. L., Schlitzer, R., Slater, R. D., Weirig, M.-F., Yamanaka, Y., and Yool, A.: Impact of circulation on export production, dissolved organic matter and dissolved oxygen in the ocean: Results from Phase II of the Ocean Carbon-cycle Model Intercomparison Project (OCMIP-2), *Global Biogeochem. Cy.*, 21, GB3007, doi:10.1029/2006GB002857, 2007. 10861, 10862, 10863

Oschlies, A., Schulz, K. G., Riebesell, U., and Schmittner, A.: Simulated 21st century's increase in oceanic suboxia by CO₂-enhanced biotic carbon export, *Global Biogeochem. Cy.*, 22, GB4008, doi:10.1029/2007GB003147, 2008. 10861

Perry, G. D., Duffy, P. B., and Miller, N. L.: An extended data set of river discharges for validation of general circulation models, *J. Geophys. Res.*, 101, 21339–21349, 1996. 10866, 10887, 10911

Sayles, F. L., Martin, W. R., Chase, Z., and Anderson, R. F.: Benthic remineralization and burial of biogenic SiO₂, CaCO₃, organic carbon, and detrital material in the Southern Ocean

Organic matter burial in global biogeochemical ocean models

I. Kriest and A. Oschlies

[Title Page](#)
[Abstract](#)
[Introduction](#)
[Conclusions](#)
[References](#)
[Tables](#)
[Figures](#)




[Back](#)
[Close](#)
[Full Screen / Esc](#)
[Printer-friendly Version](#)
[Interactive Discussion](#)

along a transect at 170° West, Deep-Sea Res. Pt. II, 48, 4323–4383, doi:10.1016/S0967-0645(01)00091-1, 2001. 10884, 10885

Schmittner, A., Oschlies, A., Matthews, H. D., and Galbraith, E. D.: Future changes in climate, ocean circulation, ecosystems, and biogeochemical cycling simulated for a business-as-usual CO₂ emission scenario until year 4000 AD, Global Biogeochem. Cy., 22, GB1013, doi:10.1029/2007GB002953, 2008. 10863

Seiter, K., Hensen, C., and Zabel, M.: Benthic carbon mineralization on a global scale, Global Biogeochem. Cy., 19, GB1010, doi:10.1029/2004GB002225, 2005. 10872, 10873, 10907

Siegel, D., Fields, E., and Buessler, K.: A bottom-up view of the biological pump: Modeling source funnels above ocean sediment traps, Deep-Sea Res., 55, 108–127, doi:10.1016/j.dsr.2007.10.006, 2008. 10877

Somes, C. J., Oschlies, A., and Schmittner, A.: Isotopic constraints on the pre-industrial oceanic nitrogen budget, Biogeosciences Discuss., 10, 3121–3175, doi:10.5194/bgd-10-3121-2013, 2013.

Stahl, H., Tengberg, A., Brunnegard, J., and Hall, P. O. J.: Recycling and burial of organic carbon in sediments of the Porcupine Abyssal Plain, NE Atlantic, Deep-Sea Res. Pt. I, 51, 777–791, doi:10.1016/S0967-0637(04)00047-0, 2004. 10884, 10886

Stammer, D., Ueyoshi, K., Köhl, A., Large, W. G., Josey, S. A., and Wunsch, C.: Estimating air–sea fluxes of heat, freshwater, and momentum through global ocean data assimilation, J. Geophys. Res., 109, C05023, doi:10.1029/2003JC002082, 2004. 10866

Stramma, L., Prince, E. D., Schmidtko, S., Luo, J., Hoolihan, J. P., Visbeck, M., Wallace, D. W. R., Brandt, P., and Koertzinger, A.: Expansion of oxygen minimum zones may reduce available habitat for tropical pelagic fishes, Nat. Clim. Change, 2, 33–37, doi:10.1038/NCLIMATE1304, 2012. 10861

Turnewitsch, R. and Springer, B. M.: Do bottom mixed layers influence ²³⁴Th dynamics in the abyssal near-bottom water column?, Deep-Sea Res. Pt. I, 48, 1279–1307, doi:10.1016/S0967-0637(00)00104-7, 2001. 10881

Vangriesheim, A., Springer, B., and Crassous, P.: Temporal variability of near-bottom particle resuspension and dynamics at the Porcupine Abyssal Plain, Northeast Atlantic, Prog. Oceanogr., 50, 123–145, doi:10.1016/S0079-6611(01)00051-9, 2001. 10881, 10882

Wallmann, K.: Phosphorus imbalance in the global ocean?, Global Biogeochem. Cy., 24, GB4030, doi:10.1029/2009GB003643, 2010. 10896

Yahel, G., Yahel, R., Katz, T., Lazar, B., Herut, B., and Tunnicliffe, V.: Fish activity: a major mechanism for sediment resuspension and organic matter remineralization in coastal marine sediments, *Mar. Ecol.-Prog. Ser.*, 372, 195–209, doi:10.3354/meps07688, 2008. 10882

5 Yool, A., Popova, E. E., and Anderson, T. R.: Medusa-1.0: a new intermediate complexity plankton ecosystem model for the global domain, *Geosci. Model Dev.*, 4, 381–417, doi:10.5194/gmd-4-381-2011, 2011. 10862

10 Yool, A., Popova, E. E., and Anderson, T. R.: MEDUSA-2.0: an intermediate complexity biogeochemical model of the marine carbon cycle for climate change and ocean acidification studies, *Geosci. Model Dev. Discuss.*, 6, 1259–1365, doi:10.5194/gmdd-6-1259-2013, 2013. 10862

**Organic matter burial
in global
biogeochemical
ocean models**

I. Kriest and A. Oschlies

Title Page

Abstract

Introduction

Conclusions

References

Tables

Figures

⏪

⏩

◀

▶

Back

Close

Full Screen / Esc

Printer-friendly Version

Interactive Discussion



Organic matter burial in global biogeochemical ocean models

I. Kriest and A. Oschlies

Title Page

Abstract

Introduction

Conclusions

References

Tables

Figures

◀

▶

◀

▶

Back

Close

Full Screen / Esc

Printer-friendly Version

Interactive Discussion

Table 2. Global benthic and boundary fluxes for scenarios “slow” to “fast” (s2 to s3) of different models, and observational estimates from Wallmann (2010), his Tables 1 (riverine P flux to ocean), 2 (burial flux in sediment) and 3 (benthic phosphate release). Identifiers for experiments different sinking exponents as in Table 1. Simulated “benthic remineralization” value estimated from total detritus remineralization in last box (see text). We also denote the RMSE of global particle flux in 2000 m, benthic remineralization and burial, as exemplified for BUR in Figs. 8, 9 and 10, respectively.

Flux, RMSE	CTL (no burial)			BUR (strong burial)			wBUR (weak burial)			DUNNE			Observations
	s2	ref	s3	s2	ref	s3	s2	ref	s3	s2	ref	s3	
Global riverine flux to the ocean [GmolPyr ⁻¹]													
Rivers	0	0	0	154	266	511	31	55	106	121	220	450	270
Global particle flux in 2000 m [GmolPyr ⁻¹]													
> 2000 m	305	455	672	304	461	707	306	458	685	304	460	705	342 ± 42 ^b
Global “benthic remineralization” [GmolPyr ⁻¹]													
Total:	446	562	748	317	350	373	419	518	673	343	385	419	1060
> 200 m	278	416	630	203	253	290	255	375	550	221	281	327	310 ^a
> 2000 m	187	305	495	134	175	208	169	268	419	148	198	237	
Global burial [GmolPyr ⁻¹]													
Total:	0	0	0	154	266	511	31	55	106	121	220	450	419
> 200 m	0	0	0	77	176	393	24	46	96	58	146	352	109 ^a
> 2000 m	0	0	0	54	134	315	19	40	85	39	111	284	
RMSE for particle flux (<i>F</i>), “benthic remineralization” (<i>R</i>) and burial (<i>B</i>) ([mmolCm ⁻² yr ⁻¹])													
<i>F</i>	112	145	258	113	149	276	112	146	264	113	148	275	
<i>R</i>	290	294	379	282	255	238	290	287	350	278	250	234	
<i>B</i>	338	338	338	283	258	305	327	322	315	294	265	287	

^a From Wallmann (2010), without “shelf and slope” region.

^b Observation of particle flux in 2000 m from Honjo et al. (2008).

Organic matter burial in global biogeochemical ocean models

I. Kriest and A. Oschlies

Table 3. Different misfit metrics, normalized by global average concentration of dissolved tracers (2.17 mmol P m⁻³ for phosphate, 174.31 mmol O₂ m⁻³ for oxygen) or by global annual flux (see Table 2), for scenarios “slow” to “fast” (s2 to s3) of different models. See text and Eq. (3) for more information.

Metric	CTL (no burial)			BUR (strong burial)			wBUR (weak burial)			DUNNE		
	s2	ref	s3	s2	ref	s3	s2	ref	s3	s2	ref	s3
I: norm. RMSE to phosphate r_P and oxygen r_O												
r_P	0.10	0.14	0.20	0.10	0.13	0.17	0.10	0.13	0.19	0.10	0.13	0.17
r_O	0.14	0.21	0.36	0.15	0.14	0.17	0.14	0.19	0.31	0.15	0.15	0.19
$\sum r_x$	0.24	0.35	0.56	0.25	0.27	0.34	0.24	0.32	0.50	0.25	0.28	0.36
II: norm. deviation from global average oxygen (global oxygen inventory, d_O)												
O ₂	-0.03	-0.15	-0.27	0.01	-0.05	-0.09	-0.02	-0.12	-0.23	0.00	-0.07	-0.11
$\sum x $	0.03	0.15	0.27	0.01	0.05	0.09	0.02	0.12	0.23	0.00	0.07	0.11
III: norm. RMSE to particle flux (r_F), “benthic remineralization” (r_R) and burial (r_B)												
r_F	0.33	0.42	0.75	0.33	0.44	0.81	0.33	0.43	0.77	0.33	0.43	0.80
r_R	0.94	0.95	1.22	0.91	0.82	0.77	0.94	0.93	1.13	0.90	0.81	0.75
r_B	3.10	3.10	3.10	2.60	2.37	2.80	3.00	2.95	2.89	2.70	2.43	2.63
$\sum r_x$	4.37	4.47	5.07	3.84	3.63	4.38	4.27	4.31	4.79	3.93	3.67	4.18
IV: norm. deviation from global runoff (d_r), particle flux (d_F), “benthic remineralization” (d_R) and burial (d_B)												
d_r	-1.00	-1.00	-1.00	-0.43	-0.01	0.89	-0.89	-0.80	-0.61	-0.55	-0.19	0.67
d_F	-0.11	0.33	0.96	-0.11	0.35	1.07	-0.11	0.34	1.00	-0.11	0.35	1.06
d_R	-0.40	-0.02	0.60	-0.57	-0.44	-0.33	-0.45	-0.14	0.35	-0.52	-0.36	-0.24
d_B	-1.00	-1.00	-1.00	-0.50	0.23	1.89	-0.83	-0.63	-0.22	-0.64	0.02	1.61
$\sum x $	2.51	2.35	3.56	1.61	1.03	4.18	2.28	1.91	2.18	1.82	0.92	3.58
Total Misfit S (sum over I-IV)												
S	7.15	7.32	9.46	5.71	4.98	8.99	6.81	6.66	7.70	6.00	4.94	8.23

Title Page

Abstract

Introduction

Conclusions

References

Tables

Figures

◀

▶

◀

▶

Back

Close

Full Screen / Esc

Printer-friendly Version

Interactive Discussion



Table 4. Latitude (° N), longitude (° W), depth (m), rain rate, remineralization and burial (all in $\text{mmol C m}^{-2} \text{yr}^{-1}$), data set Id and author/location for the data set used for regression and model assessment.

Lat	Lon	Depth	Rain Rate	Remin.	Burial	Id	Author	Location
8.80	103.75	3143	130.0	118.0	4.00	1	Ben84	M
6.54	92.81	3599	120.0	119.0	1.00	1	Ben84	H
0.02	11.74	4052		116.0	10.00	1	Ben84	EEA
1.10	138.95	4144		200.0	2.00	1	Ben84	C
11.02	140.08	4910	18.0	18.0	0.10	1	Ben84	S
33.00	119.00	1800		474.5	766.50	2	Ber87	SNicolas
33.50	118.50	900		584.0	1168.00	2	Ber87	SPedro
32.58	118.18	1904	704.0	454.0	250.00	3	Ben89	SClemente
33.37	118.42	100	1791.5	869.9	921.60	4	Jah90	SCatalina
33.75	118.83	500	1703.3	973.3	730.00	4	Jah90	SMonica
-5.00	140.00	4391	84.0	76.7	1.46	5	Ber97	EqPac5S
-2.00	140.00	4475	109.5	157.0	1.57	5	Ber97	EqPac2S
0.00	140.00	4440	138.7	157.0	1.53	5	Ber97	EqPac0N
1.00	140.00	4440	127.8	149.7	0.84	5	Ber97	EqPac1N
2.00	140.00	4540	105.9	200.8	0.99	5	Ber97	EqPac2N
5.00	140.00	4560	120.5	63.9	0.40	5	Ber97	EqPac5N
49.48	11.17	208	1595.1		13.50	6	Loh98	shelf
49.32	12.07	1021	690.9		6.57	6	Loh98	upperlope
49.13	13.22	2810	542.8		7.30	6	Loh98	lowerlope
49.04	13.70	4509	365.0		8.40	6	Loh98	PAP
-66.14	169.63	3148		135.0	1.70	7	Say01	M5
-64.20	170.10	2746		275.0	4.20	7	Say01	I5/4
-63.14	169.80	2930		185.0	4.20	7	Say01	M4
-61.88	169.97	3303		260.0	10.00	7	Say01	I4/3
-60.26	170.13	3979		61.0	1.70	7	Say01	M3
-58.69	169.98	4345		110.0	1.70	7	Say01	I3/2
-56.90	170.19	4969		31.0	0.80	7	Say01	M2
46.71	124.75	333	3249.9	2590.4	665.70	8	Dev01	Washington
22.63	106.45	445	1880.2	1342.4	505.32	8	Dev01	Mexico
48.89	16.47	4817	178.9	167.9	11.00	9	Sta04	PAP
0.02	86.46	2941			50.00	10	Kie07	ME524JC
0.10	86.48	2740			16.67	10	Kie07	Y6971P
2.60	83.99	3085	330.6*		16.67	10	Kie07	P7
-1.85	82.79	2203			33.33	10	Kie07	ME527JC
-3.60	83.95	3209			33.33	10	Kie07	TR13631
2.26	90.95	2348			8.33	10	Kie07	TR13619

* Rain rate determined from trap-derived sedimentation rate by Honjo et al. (1992).

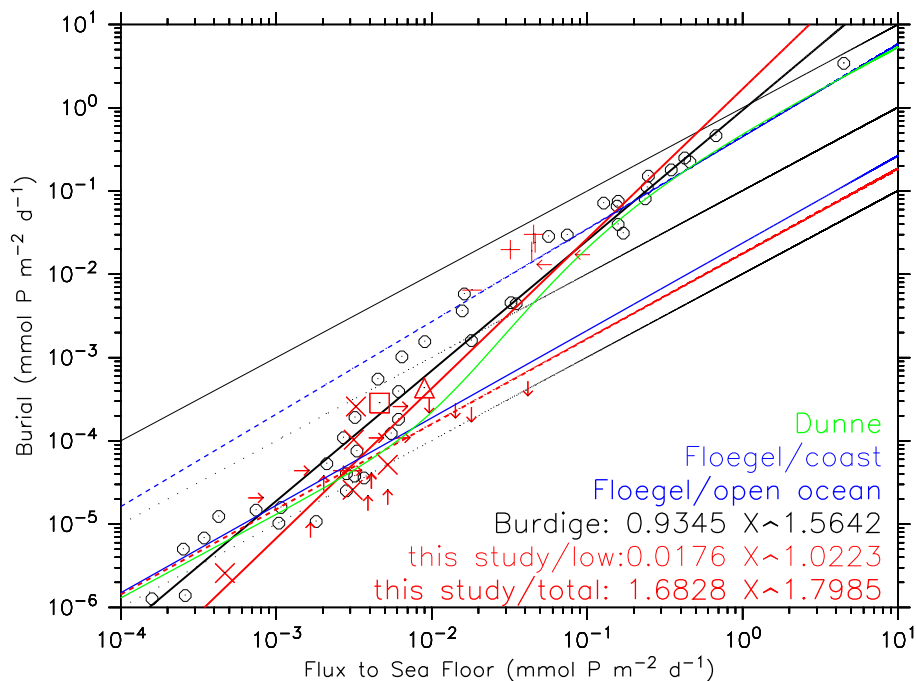


Fig. 1. Burial vs. rain rate onto sediment for various approaches. Open black circles and thick black line: observations and regression based on data set by Burdige (2007). Thick red symbols: data compilation for regions with rain rate $< 250 \text{ mmol C m}^{-2} \text{ yr}^{-1}$. Thin red symbols: data compilation for regions with rain rate $\geq 250 \text{ mmol C m}^{-2} \text{ yr}^{-1}$. Straight red line: regression for data compilation over all regions. Dashed red line: regression for data compilation over regions with rain rate $< 250 \text{ mmol C m}^{-2} \text{ yr}^{-1}$. Regressions from Flögel et al. (2011) are shown as straight (open ocean) and dashed (coastal) blue line. The algorithm by Dunne et al. (2007) is denoted as green line. Thin black lines denote constant burial efficiencies of 100 (straight), 10 and 1% (both dotted).

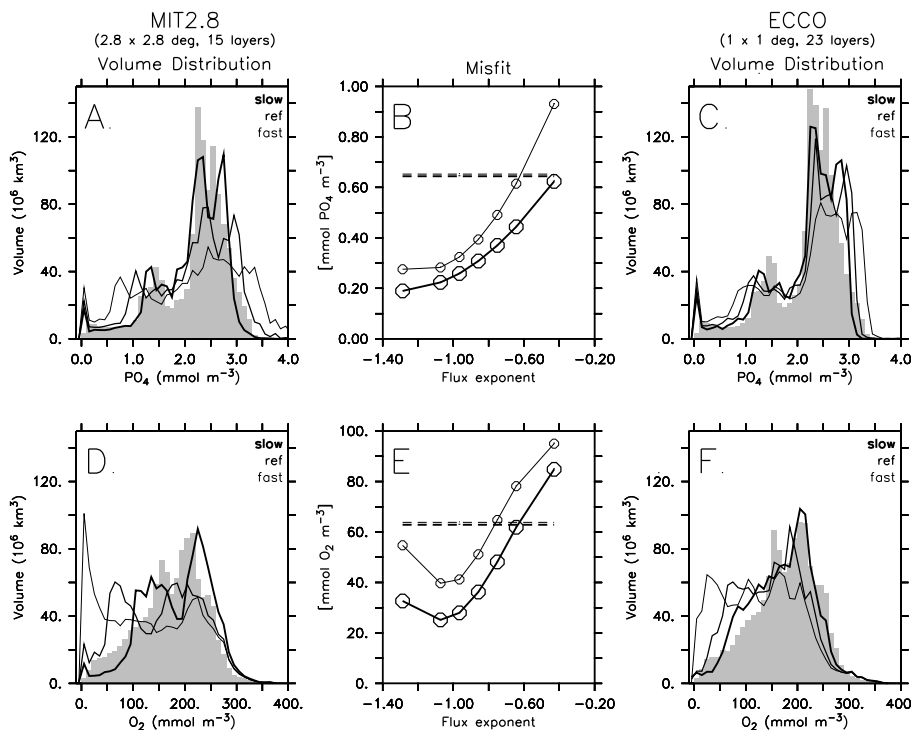


Fig. 2. Volume distributions of global phosphate (upper, **A** and **C**) and oxygen (lower, **D** and **F**) for model CTL in the MIT2.8 (left) and ECCO (right) configuration. Grey bars denote the corresponding observations (WOA05). Lines denote the different experiments. Thin lines: fast sinking profile. Thick lines: slow sinking profile. Medium line: reference scenario. Mid panel: Misfit of phosphate (upper) and oxygen (lower). Thin lines: MIT2.8 configuration. Thick lines: ECCO configuration. Horizontal lines: Global variance of observations.

Title Page

Abstract

Introduction

Conclusions

References

Tables

Figures

◀

▶

◀

▶

Back

Close

Full Screen / Esc

Printer-friendly Version

Interactive Discussion

Organic matter burial in global biogeochemical ocean models

I. Kriest and A. Oschlies

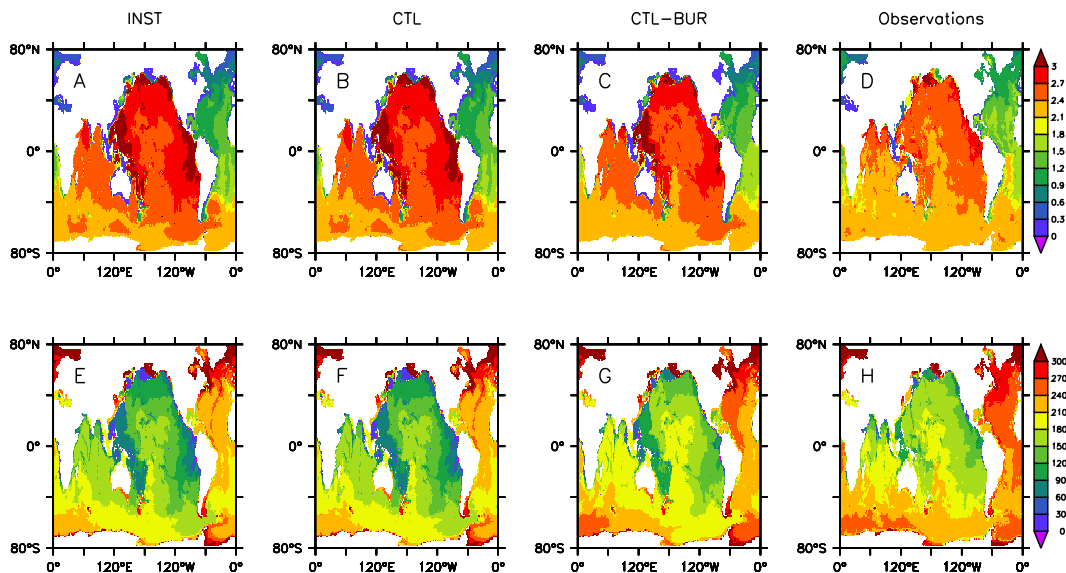


Fig. 3. Concentration of phosphate (top panels **A–D**) and oxygen (bottom panels **E–H**) in the deepest model box above the hypothetical sediment, for models INST (**A, E**), CTL (**B, F**), BUR (**C, G**) and from observations (**D, H**, Garcia et al., 2006a,b).

[Title Page](#)

[Abstract](#)

[Introduction](#)

[Conclusions](#)

[References](#)

[Tables](#)

[Figures](#)

⏪

⏩

◀

▶

[Back](#)

[Close](#)

[Full Screen / Esc](#)

[Printer-friendly Version](#)

[Interactive Discussion](#)

Organic matter burial in global biogeochemical ocean models

I. Kriest and A. Oschlies

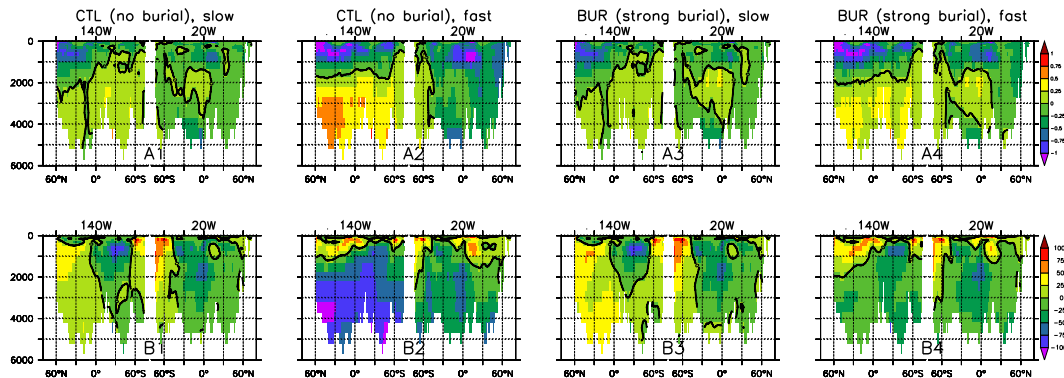


Fig. 4. Model mismatch (model – observation) for phosphate (upper panels; “A”) and oxygen (lower panels; “B”) plotted along sections for different model experiments CTL (slow sinking: **A1**, **B1**; fast sinking: **A2**, **B2**), and BUR (slow: **A3**, **B3**; fast: **A4**, **B4**). Sub-panels on the left show north-south section along 140° W. Sub-panels on the right show south-north section along 20° W.

[Title Page](#)
[Abstract](#)
[Introduction](#)
[Conclusions](#)
[References](#)
[Tables](#)
[Figures](#)
[Back](#)
[Close](#)
[Full Screen / Esc](#)
[Printer-friendly Version](#)
[Interactive Discussion](#)

Organic matter burial in global biogeochemical ocean models

I. Kriest and A. Oschlies

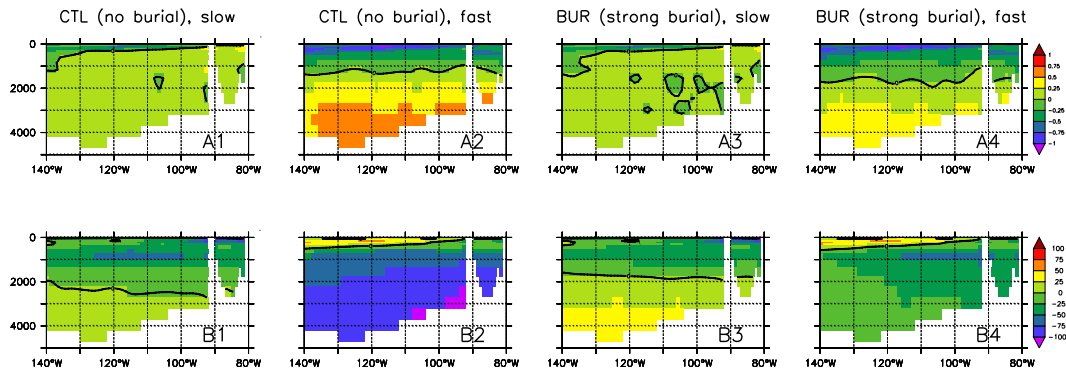


Fig. 5. Model mismatch (model – observation) for phosphate (upper panels; “A”) and oxygen (lower panels; “B”) plotted along the equator from 140° W to the coast of Ecuador for different model experiments CTL (slow sinking: **A1**, **B1**; fast sinking: **A2**, **B2**), and BUR (slow: **A3**, **B3**; fast: **A4**, **B4**).

[Title Page](#)
[Abstract](#)
[Introduction](#)
[Conclusions](#)
[References](#)
[Tables](#)
[Figures](#)
[⏪](#)
[⏩](#)
[◀](#)
[▶](#)
[Back](#)
[Close](#)
[Full Screen / Esc](#)
[Printer-friendly Version](#)
[Interactive Discussion](#)

Organic matter burial in global biogeochemical ocean models

I. Kriest and A. Oschlies

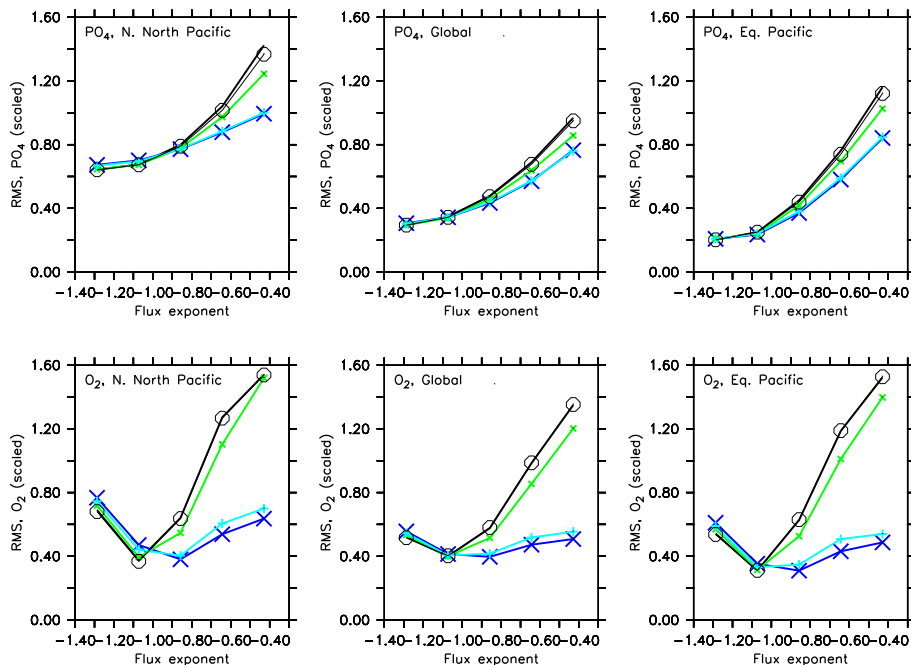


Fig. 6. Misfit function, calculated as RMSE, divided by observed global standard deviation, for phosphate (upper panels) and oxygen (lower panels). Left: Misfit for northern North Pacific (north of 40° N). Right: misfit for eastern equatorial Pacific (between $\pm 10^{\circ}$ and east of 140° W). Middle: global misfit. Black lines: CTL; Thin black lines with open circles: INST; Green small crosses and lines: WBUR; Blue large crosses and lines: BUR. Turquoise pluses and lines: DUNNE.

[Title Page](#)
[Abstract](#)
[Introduction](#)
[Conclusions](#)
[References](#)
[Tables](#)
[Figures](#)
[Back](#)
[Close](#)
[Full Screen / Esc](#)
[Printer-friendly Version](#)
[Interactive Discussion](#)

Organic matter burial in global biogeochemical ocean models

I. Krist and A. Oschlies

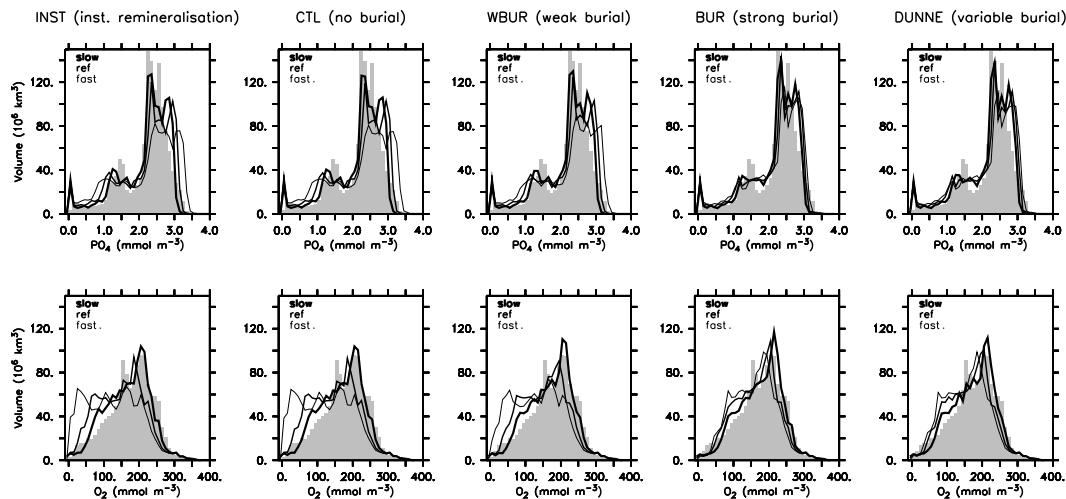


Fig. 7. Volume distributions of global phosphate (upper panels) and oxygen (lower panels) for different model experiments. Grey bars denote the corresponding observations (WOA05). Lines denote the different experiments. Thin lines: fast sinking profile. Thick lines: slow sinking profile. Medium lines: reference scenario.

Title Page

Abstract

Introduction

Conclusions

References

Tables

Figures

⏪

⏩

◀

▶

Back

Close

Full Screen / Esc

Printer-friendly Version

Interactive Discussion

Organic matter burial
in global
biogeochemical
ocean models

I. Krist and A. Oschlies

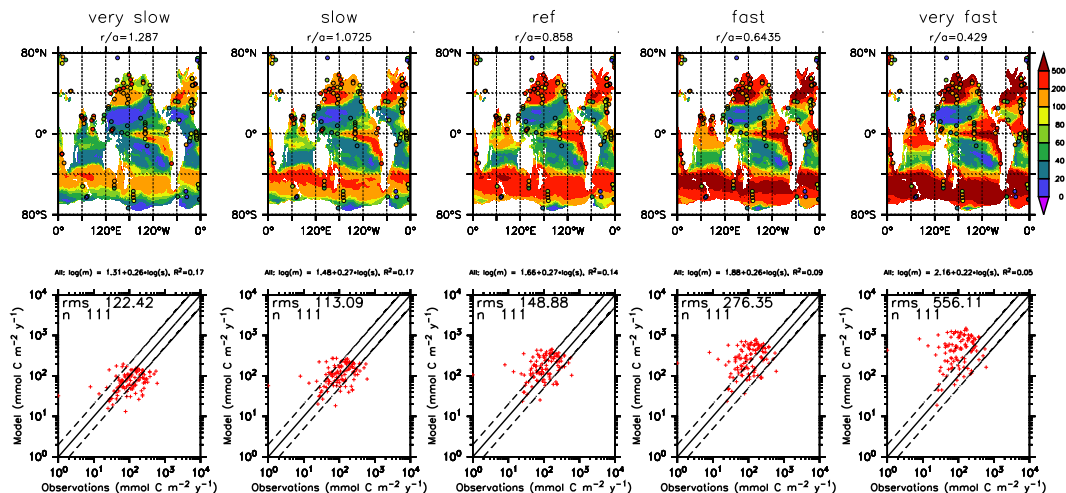


Fig. 8. Upper panels: particle flux in 2000 m, for experiment BUR with burial, and observations. Sinking speed in models increases from the left (slow) to the right (fast). Small colored circles denote observations from the data set by Honjo et al. (2008), on the same color scale as the model results. Lower panels: Simulated vs. observed particle flux. Lines indicate 1 : 2, 1 : 1 and 2 : 1 relationship. The panels also denote the RMSE of the modeled vs. observed flux, as well as the number of data points sampled.

Title Page

Abstract

Introduction

Conclusions

References

Tables

Figures



Back

Close

Full Screen / Esc

Printer-friendly Version

Interactive Discussion

Organic matter burial
in global
biogeochemical
ocean models

I. Krist and A. Oschlies

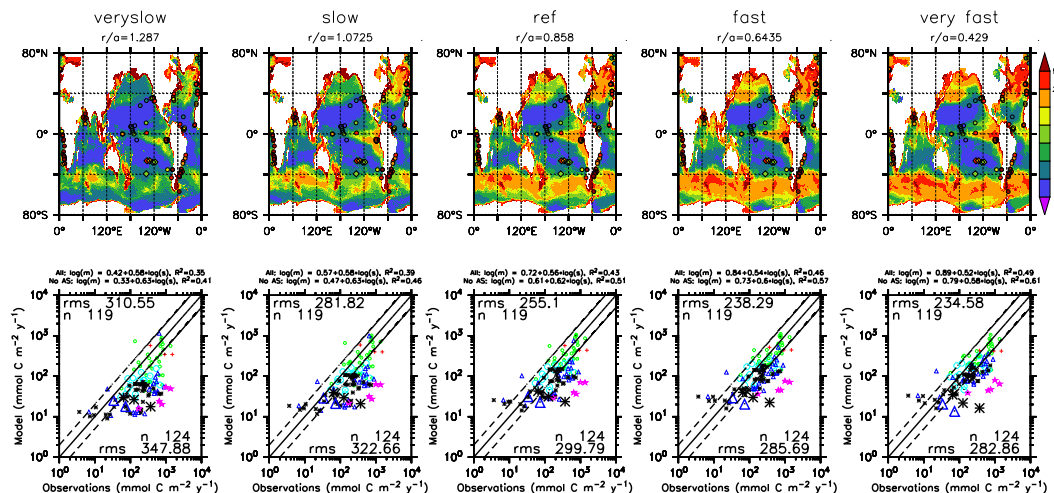


Fig. 9. Upper panels: Benthic remineralization (see text) for experiment BUR with burial, and observations. Flux exponent in models decreases from the left (slow) to the right (fast). Colored symbols denote observations from the data set by Seiter et al. (2005, circles) and Fischer et al. (2009, diamonds), on the same color scale as model results. Lower panels: Simulated vs. observed benthic remineralization. Different colors and symbols denote different depths and/or data types: green small circles: 1000–2000 m. Turquoise large circles: 2000–3000 m. Blue triangles: 3000–4000 m. Black crosses: > 4000 m. Pink stars: Arabian Sea (> 3000 m). Data by Fischer et al. (2009, South Pacific) are denoted by large blue triangles (3000–4000 m) and large black crosses (> 4000 m). The panels also denote the RMSE of the modeled vs. observed benthic remineralization (data set by Seiter et al., 2005), and the number of data points sampled (upper numbers: without Arabian Sea data, lower numbers: total data set).

Title Page

Abstract

Introduction

Conclusions

References

Tables

Figures

◀

▶

◀

▶

Back

Close

Full Screen / Esc

Printer-friendly Version

Interactive Discussion

Organic matter burial in global biogeochemical ocean models

I. Kriest and A. Oschlies

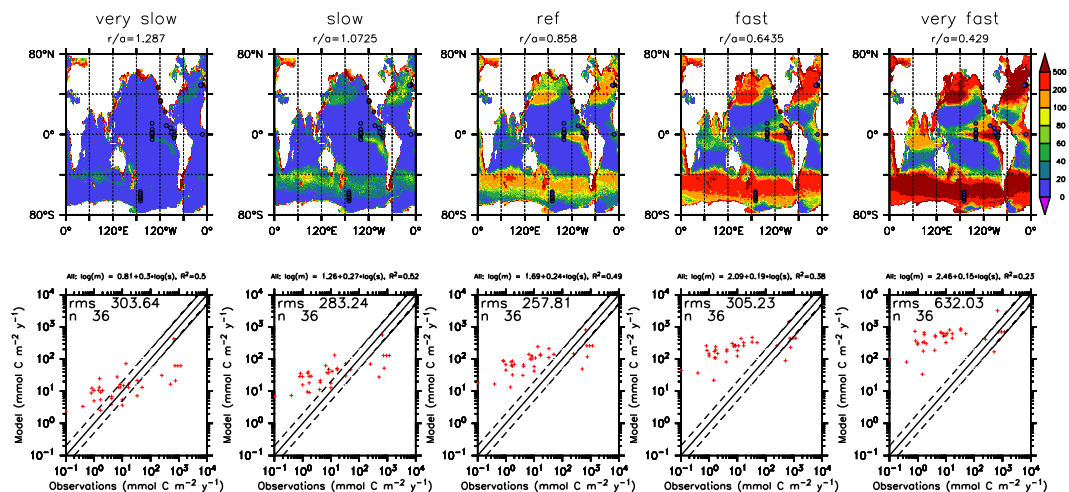


Fig. 10. Upper panels: Burial in the sediment (see text), for experiment BUR with burial, and observations. Flux exponent in models decreases from the left (slow) to the right (fast). Colored circles denote observations in the same colour scale as model results (see text and Appendix A). Lower panels: Simulated vs. observed burial in the sediment. Lines indicate 1 : 2, 1 : 1 and 2 : 1 relationship. The panels also denote the RMSE of the modeled vs. observed DOU, and the number of data points sampled.

[Title Page](#)
[Abstract](#)
[Introduction](#)
[Conclusions](#)
[References](#)
[Tables](#)
[Figures](#)

[Back](#)
[Close](#)
[Full Screen / Esc](#)
[Printer-friendly Version](#)
[Interactive Discussion](#)

Organic matter burial
in global
biogeochemical
ocean models

I. Kriest and A. Oschlies

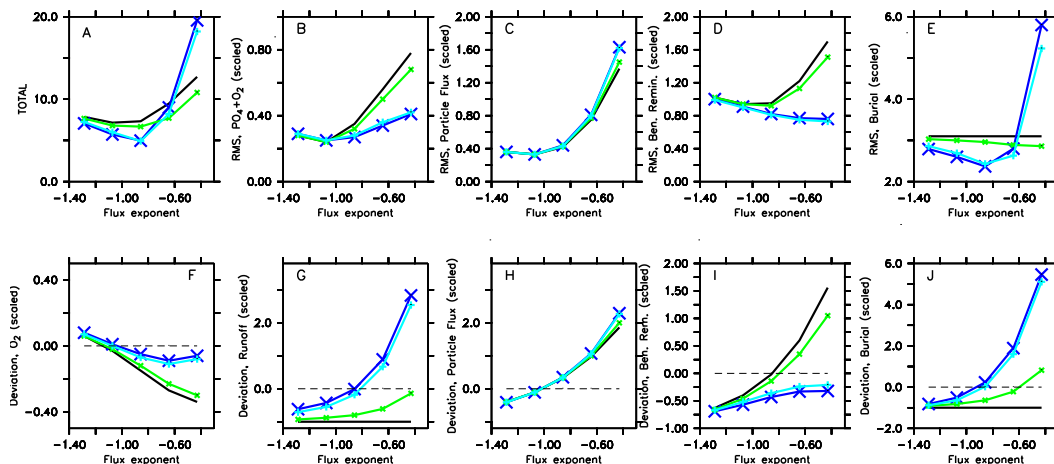


Fig. 11. Metrics for different model types plotted vs. different sinking speed. Panel B: sum of misfit (RMS, divided by observed global average concentration) for phosphate and oxygen; Panels (C–E): normalized misfit to data sets for particle flux in 2000 m (C), benthic remineralization (D), benthic burial (E). Bottom panels (F–J): normalized deviation between simulated and observed global inventory of oxygen (F), between global fluxes of organic particles (H), benthic remineralization (I), benthic burial (J) and global river runoff of phosphate (G). (A) shows the sum over all panels (B) to (J). Normalization of biogeochemical fluxes has been carried out by global integrated fluxes listed in Table 2. Colours as in Fig. 6.

Title Page

Abstract

Introduction

Conclusions

References

Tables

Figures

◀

▶

◀

▶

Back

Close

Full Screen / Esc

Printer-friendly Version

Interactive Discussion

Organic matter burial in global biogeochemical ocean models

I. Krist and A. Oschlies

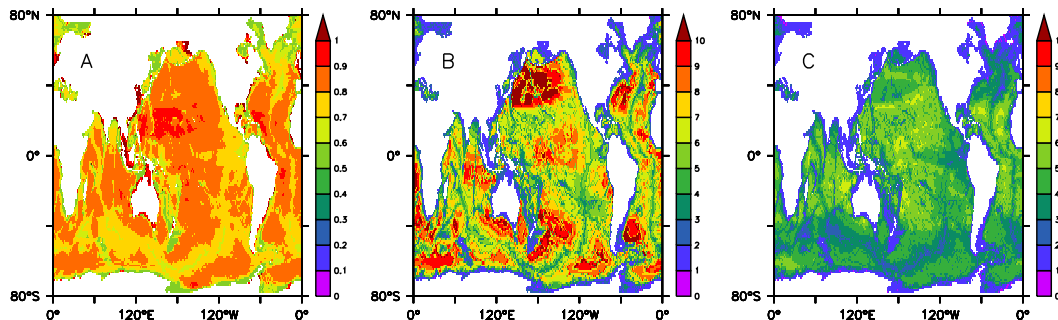


Fig. 12. Detritus concentration in the bottom layer of reference scenarios models INST **(A)**, CTL **(B)**, and BUR **(C)**, expressed as multiple of detritus concentration the layer above. Note the different colour scales.

[Title Page](#)[Abstract](#)[Introduction](#)[Conclusions](#)[References](#)[Tables](#)[Figures](#)[⏪](#)[⏩](#)[◀](#)[▶](#)[Back](#)[Close](#)[Full Screen / Esc](#)[Printer-friendly Version](#)[Interactive Discussion](#)

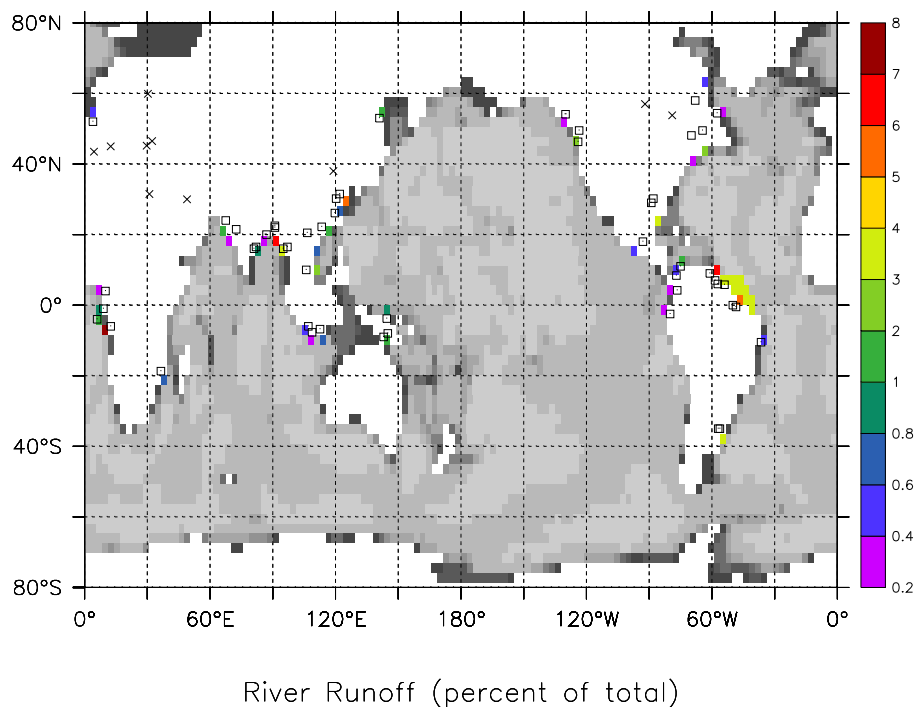


Fig. 13. Distribution of river runoff (as fraction of total runoff, coloured boxes), as calculated from Perry et al. (1996) for rivers south of 60° N and mapped onto the topography of the MIT2.8 degree model as described in the text. Symbols denote original locations from the data set by Perry et al. (1996). Crosses: omitted from runoff calculation (see text). Open squares: included in runoff calculation.

Title Page

Abstract

Introduction

Conclusions

References

Tables

Figures



Back

Close

Full Screen / Esc

Printer-friendly Version

Interactive Discussion